The Pennsylvania State University

The Graduate School

Department of Energy and Geo-Environmental Engineering

OPTIMIZATION OF RECOVERY FROM TWO-LAYER RESERVOIRS WITH CROSSFLOW

A Thesis in

Petroleum and Natural Gas Engineering

by

Eric John Kuhl

Submitted in Partial Fulfillment
of the Requirements
for the Degree of

Master of Science

December 2003

Eric Kuhl

The thesis of Eric Kuhl was reviewed and approved* by the following:

Turgay Ertekin
Head of Graduate Program
Professor of Petroleum and Natural Gas Engineering and George E. Trimble Chair in Earth and Mineral Sciences
Thesis Advisor

Peter B. Flemings
Associate Professor of Geosciences

Michael Adewumi
Professor of Petroleum and Natural Gas Engineering

*Signatures are on file in the Graduate School

Abstract

Producing from both layers of two-layer reservoirs with crossflow can result in bypassed reserves in the laminated layer depending on the permeabilities and thickness of each layer. In the case of the RM reservoir of the Popeye field this is a significant amount of reserves (32 BCF). An optimization protocol is developed using a simple model to determine if perforating only the laminated layer of two-layer reservoirs with crossflow increases the recovery from the field. The optimization protocol accounts for lower well rates when only the laminated layer is perforated by discounting recoveries based on how far into the future they are recovered. The validity of the optimization protocol is tested using simulations of the Popeye field. These simulations showcase both where the protocol is accurate and what aspects of the protocol could be improved.

Table of Contents

List of Figures

List of Tables

Preface

This thesis is composed of an introductory chapter, two primary research chapters and three appendices. The two primary research chapters focus on developing an optimization protocol that determines which perforation strategy recovers the most hydrocarbons from two-layer reservoirs with crossflow and the application of this protocol to a gas condensate field in the Gulf of Mexico. Chapter one, Introduction and Problem Statement" focuses on introductory concepts that surround the topics discussed in the majority of the thesis and develops the questions the thesis research intends to cover. Chapter two, "Optimization of Recovery from Two-layer Reservoirs with Crossflow" contains an in depth discussion of how recovery can be increased from two-layer reservoirs with crossflow depending on the horizontal permeability, the vertical permeability, and the thickness of the two layers within the reservoir. Chapter three, "Optimization of Recovery from the Popeye Reservoir" showcases the abilities of the optimization protocol developed in Chapter 3 to predict the optimal perforation strategy for the Popeye reservoir.

Both Appendix A and B include information crucial to reproducing the simulation results displayed within this thesis. Appendix A contains supplemental input data required to perform simulations for the Popeye field. The specific values and/or curves used for capillary pressure, relative permeability, porosity, compaction, fluid behavior, and gas-water contacts are shown here. Appendix B is composed of a table that includes the values of vertical permeability, horizontal permeability and layer thicknesses used in each simple model simulation; these simulations create the optimization protocol.

Appendix C is the paper “Integration of Geologic Model and Reservoir Simulation, Popeye Field, Green Canyon 116”. This is a collaborative effort between the members of the Petroleum Geosystems Initiative Team 2. This paper describes many of the geologic aspects of the Popeye field and some simulations that were performed to determine the effects of geologic uncertainties on simulation results. This paper is included because it supplements a lot of the geologic information used to create the Popeye reservoir model.

Acknowledgements

I am taking this opportunity to thank some of the people that have made my experience at Penn State one of the best ever. I need to first thank the many people at Shell Exploration and Production Company who have been instrumental in helping fund the Geosystems Initiative. I also want to specifically thank Dick Eikmans and Dave Miller for there mentoring before, during and after my internship with Shell.

My experience at Penn State could not have been possible without the advice and direction that I received from Dr. Flemings and Dr. Ertekin. They were always there to help with any problem and I truly felt that they had a desire for me to succeed. In addition, Dr. Adewumi and Luis Ayala were always around to help when Dr. Ertekin and Dr. Flemings were unavailable.

During my research there were countless data issues and miscellaneous problems. Luckily, Stefanie McCormick, Heather Johnson, and Rachel Altemus were always equal to the task. They always were able to make things that would take me days or weeks only take a couple hours. The same can be said for Tom Canich who was always willing to help and coach my computer illiterate self. I think he even taught me a thing or two that I might retain.

The group of people that made it the easiest to go to work each day was my officemates. I will always be indebted to Ben Seldon, Beth Strickland, and Christine (Tin-wai) Lee for the great work environment they helped create. Our office may not have always been the most productive but it was a place that ideas were freely shared and

knowledge of all aspects of life was gained. These three people alone made my experience at Penn State worth while.

The last person to thank is my fiancée, Amanda. During the entire time I spent at Penn State she was a necessary distraction. She has always motivated me to think and work outside the box. She also has been a constant source of encouragement and support. I am really looking forward to our future together and can't wait to start the next chapter in our lives.

Chapter 1

Introduction and Problem Statement

This study defines a two-layer reservoir with crossflow as a gas condensate reservoir with a laminated facies and a massive facies in direct vertical contact away from the wellbore (Fig 1.1). The two distinct facies each have different horizontal (k_h) and vertical permeabilities (k_v). In addition, the horizontal and vertical permeabilities of the laminated layer are less than the horizontal and vertical permeabilities of the massive layer, respectively. Along with the difference in permeabilities, there is a difference in relative permeability curves, porosity and capillary pressure curves.

Depositional processes can lead to the deposition of sands with a two-layer architecture that results in a crossflowing system (e.g. Fig. 1.1). Prather et al. (1998) suggest that in the Gulf of Mexico, a transition from processes that fill accommodation space to processes that bypass already filled accommodation space results in ponded facies assemblages (*PFA*) that are composed of interbedded sands and silts covered by bypass facies assemblages (*BFA*). The transition from *PFA* deposits to *BFA* deposits results in a two-layer architecture.

The J-sand of the Ram-Powell field contains both massive sand (*PFA*) and laminated sand (*BFA*) in a high energy amalgamated channel and sheet sand complex (Lerch et al., 1996). The G-sand at Popeye (Appendix C) is similar in architecture.

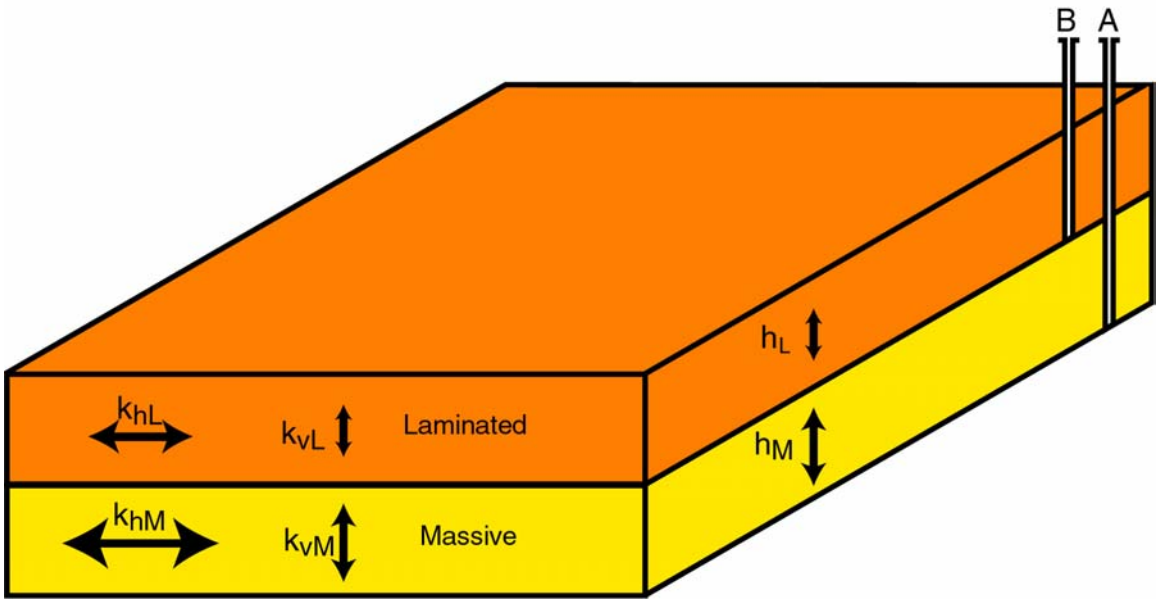

Figure 1.1: Description of two-layer, reservoir with crossflow. Each layer has its own k_h and k_v. The difference between perforating only the laminated layer (B) and perforating both layers (A) is shown.

Reservoir simulation allows for the modeling of complex interactions that take place in hydrocarbon reservoirs through time. It is used for the prediction of future reservoir performance, reserve estimation, and evaluation of past reservoir performance (Harris, 1975; Warner et al., 1979). Reservoir simulation is a fast and reliable method for predicting reservoir performance (Mattax and Dalton, 1990).

This investigation uses reservoir simulation to study many aspects of two-layer reservoirs with crossflow. Reservoir simulation is used to illustrate why producing from both layers of two-layer reservoirs with crossflow results in bypassed reserves in the laminated layer. There is also a discussion on how various reservoir properties affect the amount of reserves bypassed in the laminated layer of two-layer reservoirs with crossflow. In addition, simulations were performed to determine the best perforation strategies for this class of reservoirs depending on the horizontal permeability ratio

between the two layers (k_{hL}/k_{hM}), the vertical permeability ratio between the two layers (k_{vL}/k_{vM}) and the net thickness ratio between the two layers (h_L/h_M). An optimization protocol compiles the results of simulations performed with different perforation strategies to determine which perforation strategy recovers more hydrocarbons. The optimization protocol results are expanded to look at the economic impact of the different production strategies.

The Popeye reservoir is an example of a two-layer reservoir with crossflow. A history match is performed to calibrate a Popeye reservoir model. Once calibrated, the Popeye reservoir model is used to test the predictions of the optimization protocol. The economics model used on optimization protocol results is also tested using results from the Popeye simulations. The comparison of the optimization protocol results with the Popeye simulation results illuminate areas of weakness within the optimization protocol.

References

Harris, D. G., 1975, The Role of Geology in Reservoir Simulation Studies: Journal Of Petroleum Technology, v. 27, p. 625-632.

Lerch, C. S., K. W. Bramlett, W. H. Butler, J. N. Scales, T. B. Stroud, and C. A. Glandt, 1996, Integrated 3D reservoir modeling at Ram/Powell Field: A turbidite deposit in the eastern Gulf of Mexico: 1996 Society of Petroleum Engineers Annual Technical Coference and Exhibition.

Mattax, C. C., and R. L. Dalton, 1990, Reservoir Simulation: Journal of Petroleum Technology, v. SPE 20399, p. 692 - 695.

Prather, B. E., J. R. Booth, G. S. Steffens, and P. A. Craig, 1998, Classification, lithologic calibration, and stratigraphic succession of seismic facies of intraslope basins, deep-water Gulf of Mexico: AAPG Bulletin, v. 82, p. 701-728.

Warner, H. R. J., J. H. Hardy, N. Robertson, and A. L. Barnes, 1979, University Block 31 Field Study: Part 1 - Middle Devonian Reservoir History Match: Journal Of Petroleum Technology, v. 31, p. 962-979.

Chapter 2

Optimization of Recovery from Two-layer Reservoirs with Crossflow

Overview

Simulations using a simple system are used to illustrate explicitly the flow characteristics of two-layer reservoirs with crossflow. Also included is a description of how and where reserves are bypassed if both layers of two-layer reservoirs with crossflow are perforated. Simulations using the simple system are made that vary the vertical permeability, horizontal permeability and thickness of each layer. An optimization protocol uses these simulations to determine which perforation strategy recovers more hydrocarbons depending on the combination of permeabilities and sand thickness. Both the difference in total field recovery and a discounted recovery difference that considers the time value of money are used to determine which perforation strategy is the best for the reservoir.

Introduction

Reservoir simulation is used to predict future recovery from a field and to test various production strategies with the purpose of optimizing recovery. Studies have been performed to evaluate how to increase recovery using waterflood (Bilozir and Frydl, 1989; Van Kirk, 1976), gas injection (Zambrano et al., 1968) and infill drilling (Bayat and Tehrani, 1985).

Reservoir simulation is also used to improve geologic understanding and/or to understand how varied geologic properties affect field recovery in Gulf of Mexico turbidite reservoirs. At Mensa, integration of engineering data into reservoir simulations further refined the geologic model (Pfeiffer et al., 2000) leading to improved prediction of reservoir performance. Simulations at Popeye (Appendix C) and Ram/Powell (Lerch et al., 1996) varied structural and reservoir characteristics to determine their effect on field recovery.

In this study, reservoir simulation is used to understand the flow characteristics and the geologic properties that control the flow characteristics of two-layer reservoirs with crossflow. In addition, this study investigates how recovery from two-layer reservoirs with crossflow can be optimized for changes in the horizontal permeability, vertical permeability and thickness of the two layers. Finally, the economic impact of lower well rates from wells perforated in only the laminated layer on field recovery is considered.

Simple System

A simple system is modeled to explain behavior in a two-layer reservoir with crossflow. The model is a three-dimensional model (25 x 25 x 2 grid blocks) and consists of a laminated layer of constant thickness that overlies a massive layer of constant thickness (Fig. 2.1). Grid blocks are 250 ft by 250 ft (x and y) and the combined thickness of both layers is 200 ft. Individual layer thicknesses are constant within each layer but vary based on the ratio of laminated (h_L) to massive (h_M) sand thicknesses being examined (Table 2.1A). The depth at the center of grid block (1, 1, 1) is 11,500 ft and the depth to the center of the other grid blocks is calculated using the individual layer

thicknesses and a 4˚ dip in both the *x* and *y* directions (Fig. 2.1). The 12,160 ft original gas water contact (OGWC) (Fig 2.1) is assigned so that the ratio of initial-water-in-place to initial-pore volume is approximately equal to the same ratio in Popeye simulations (Chapter 4). Each layer of the simple model has a homogenous porosity (Table 2.2) and net-to-gross ratio (Table 2.2). The relative permeability curves (Figs A-2 and A-3), fluid properties (Table A-2), compaction model (Table A-1) and capillary pressure curves (Fig. A-4) used for the simple system are taken from the Popeye reservoir model (Appendix A). The horizontal permeability and vertical permeability is constant in each layer but varies between simulations (Table 2.1). A vertical production well is placed at the center of grid block (2, 2) and perforated in both layers or only the laminated layer depending on the production strategy being tested (Fig. 1.1).

The specified gas rate of the producing well is set so the well produces at maximum rate. Producing at the maximum rates allow us to consider the economic implications of diminished well capacity when only the laminated layer is perforated. The maximum rate for the well is achieved by specifying an unreasonably high flow rate and using a drawdown constraint of 300 psi to limit the amount of production from the well (Table 2.3). The drawdown constraint limits the amount of pressure differential between the perforated interval of the wellbore and the grid block the well penetrates. The drawdown constraint prevents the simulation from using an unreasonable pressure differential across the sand face and controls the gas flow rate from each well. Additionally, a bottom-hole pressure constraint of 1200 psi is specified as the abandonment condition for the producing well.

(A)

Net Thicknesses		
h_L	h_M	h_L/h_M
28.57	171.43	0.1
90.91	109.09	0.5
125.00	75.00	1.0
142.86	57.14	1.5
153.85	46.15	2.0

(B)

Horizontal Permeabilities		
k_{hL}	k_{hM}	k_{hL}/k_{hM}
25	1200	0.02
75	1200	0.06
125	1200	0.10
250	1200	0.21
500	1200	0.42
720	1200	0.60
1000	1200	0.83

(C)

Vertical Permeabilities		
k_{vL}	k_{vM}	k_{vL}/k_{vM}
1	500	0.002
0.4	500	0.0008
0.2	500	0.0004
0.05	500	0.0001
0.025	500	0.00005

Table 2.1: Ratios of (A) h_L/h_M, (B) k_{hL}/k_{hM}, and (C) k_{vL}/k_{vM} used in simple simulations of the optimization protocol. Also included are the actual reservoir property values used to calculate each of the ratios. These are the only properties varied in the simple model; everything else is the same between models. Each two-dimensional contour plot of the optimization protocol combines recovery difference (*RD*) results from simulations performed with one value of k_{vL}/k_{vM} (C) and all the possible combinations of h_L/h_M (A) and k_{hL}/k_{hM} (B).

Layer	Porosity (%)	k_h (mD)	k_v (mD)	Sw_{irr}	Sg_r	Net to Gross Ratio
Laminated	25	500	0.1	0.143	0.021	0.6
Massive	30	1200	500	0.119	0.022	1.0

Table 2.2: Constant property values assigned to laminated and massive layers of the simple system.

Well Constraints	
Bottom Hole Pressure	1200 psia
Draw Down	300 psia

Table 2.3: Well constraints used to control production for simple simulations. These constraints are similar to the shut-in condition for wells in the Popeye field.

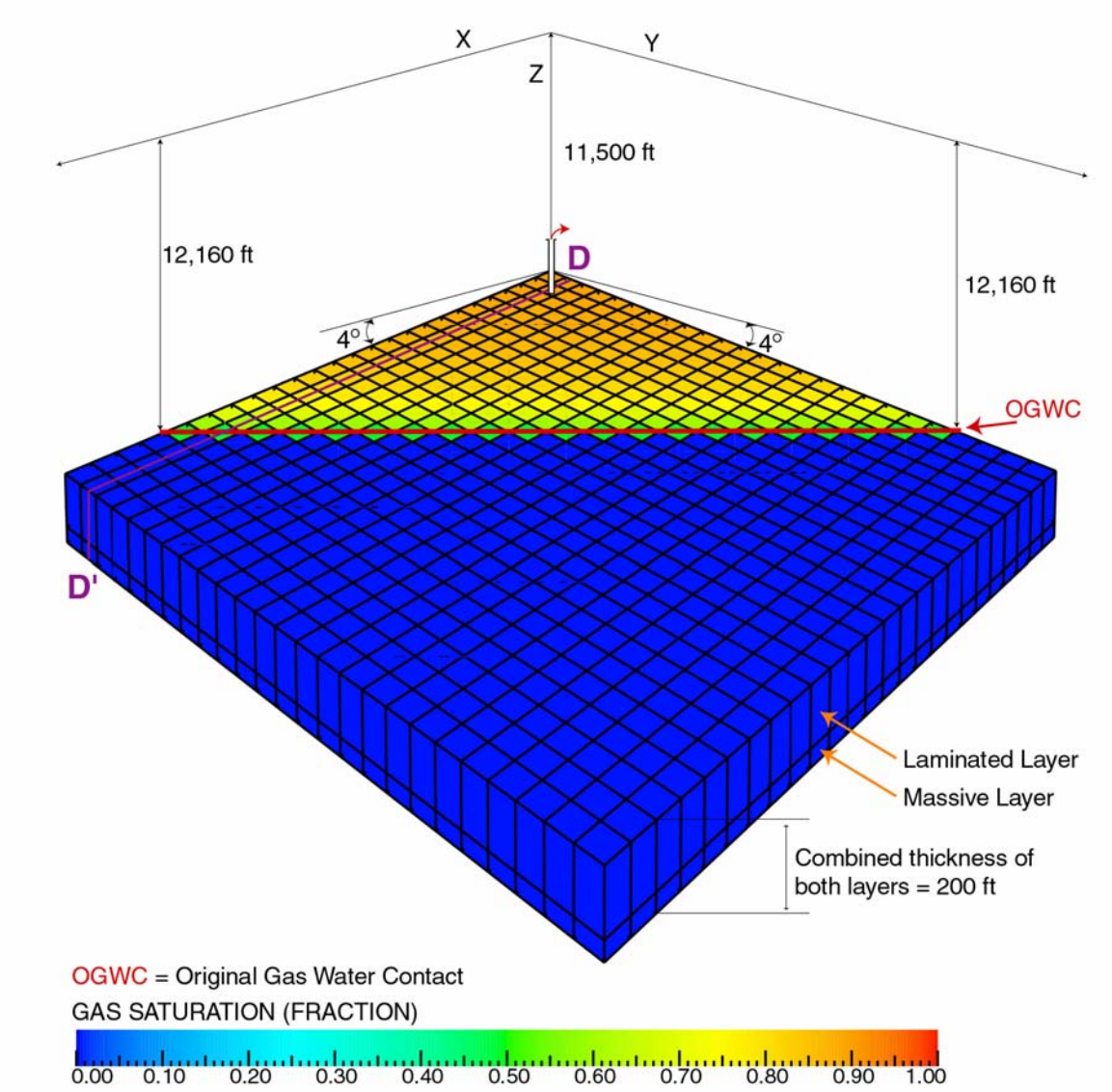

Figure 2.1: Initial gas saturation and description of the simple model. Depth to grid block (1, 1, 1) and the OGWC are noted. Cross-section D-D' is displayed at various time steps and for different properties in Figures 5.2, 5.3, and 5.5. All simple system simulations, including the optimization protocol simulations, are run using this simple model. The only input variables that are ever change in this model are k_{hL}, k_{vL} and h_L.

Flow Characteristics

To illustrate the flow characteristics of two-layer reservoirs with crossflow, a simulation was performed with k_{hL}/k_{hM} equal to 0.42, k_{vL}/k_{vM} equal to 0.0001 and h_L/h_M equal to 2.0. Both layers of the reservoir are perforated during simulation.

During production, the GWC in the laminated (top) portion of the reservoir does not move laterally as fast as the GWC in the massive layer (Fig. 2.2). Once the water in the massive layer reaches the wellbore, the remaining reserves in the laminated layer are bypassed (Fig. 2.2C).

The contrast in horizontal permeabilities (k_{hL}/k_{hM}) is one of the primary controls on how much of the reserves in the laminated layer can be produced before the massive layer waters out. The horizontal pressure gradients in each layer are about equal after 547 days of production (Fig. 2.4A). However, the difference in permeabilities (k_{hL} = 500 mD, k_{hM} = 1200 mD) results in higher horizontal gas fluxes in the massive layer then in the laminated layer (Fig 2.3B). The difference in horizontal gas fluxes makes the GWC of the massive layer reach the wellbore before all of the reserves in the laminated layer are produced (Fig. 2.2).

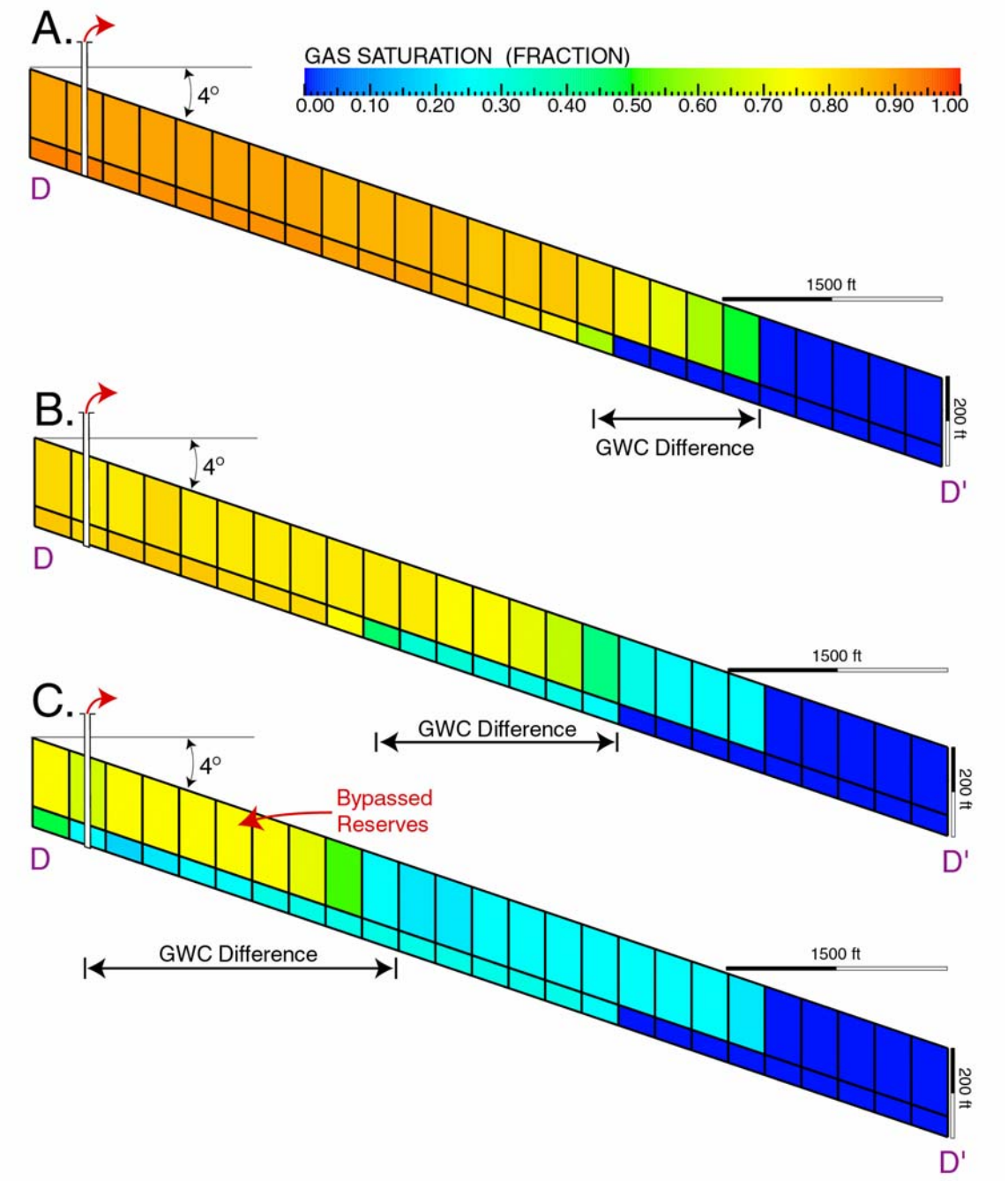

Figure 2.2: Cross-sections D-D' (Fig. 2.1) showing gas saturation through time, (A) initial, (B) 547 days after production began and (C) final (1094 days) for simple system 130 (red, Table B-1) . The difference in GWC between the laminated and massive layer is highlighted at each time step. Figure 2.3 contains a plot and cross-sections of additional fluid properties for the same cross-section at 547 days (B).

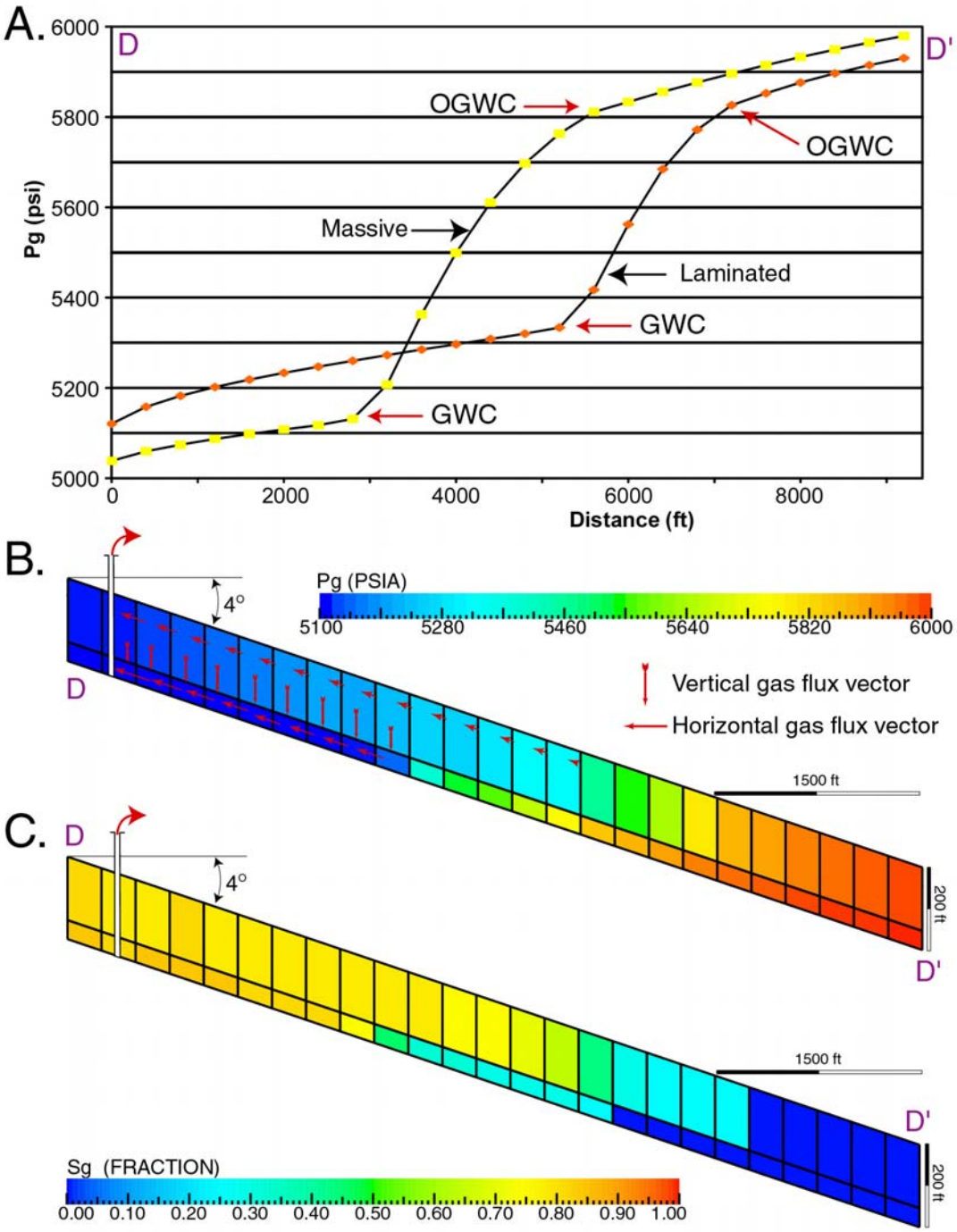

Figure 2.3: (A) Grid block gas pressure (Pg) (547 days) versus distance away for the wellbore in both the laminated and massive layers for cross-section D-D' (Fig. 2.1). (B) Cross-section D-D' (Fig. 2.1) of Pg after 547 days of simulation. Vertical and horizontal gas flux vectors are shown. The magnitude of a horizontal gas flux vector is 5000 times greater then that of a vertical gas flux vector of the same length. The horizontal gas flux arrows in the massive layer (bottom) are longer then the horizontal gas flux vectors in the laminated layer (top) signifying that the horizontal gas flux in the laminated layer is higher. (C) Cross-section D-D' (Fig. 2.1) shows gas saturation (Sg) after 547 days. After 547 days of production the reservoir has produced 164 BCF. These results are taken from simple system 130 (red, Table B-1)

The vertical potential gradients create crossflow between the two layers (Fig 2.3B). During production, for massive layer grid blocks above the massive layer GWC, gas flows from the laminated layer into the massive layer and then laterally through the massive layer to the wellbore. This adds to the amount of reserves that can be produced from the massive layer and delays the encroachment of water in the massive layer. In this case the crossflow is not enough to compensate for the difference in gas flux between the massive and laminated layers and reserves are still bypassed (Fig. 2.2C).

Properties that Control Amount of Bypassed Reserves

Simulations performed with both layers of the simple system perforated are resented to show the effect of changing k_{hL}/k_{hM}, k_{vL}/k_{vM} and h_L/h_M (Figs. 2.4 and 2.5, Table 2.4) on the amount of reserves bypassed in the laminated layer. Cases discussed include increasing k_{hL}/k_{hM}, k_{vL}/k_{vM} and h_L/h_M individually while the other two ratios are kept constant (Table 2.4). However, decreasing the ratios of the compared cases would have the opposite effect on the amount of bypassed reserves.

Ratio	Case 1	Case 2	Case 3	Case 4	Case 5	Case 6
k_{hL}/k_{hM}	0.21	0.42	0.21	0.21	0.21	0.21
k_{vL}/k_{vM}	0.0004	0.0004	0.0004	0.0008	0.0004	0.0004
h_L/h_M	1.0	1.0	1.0	1.0	1.0	2.0

Table 2.4: Values for k_{hL}/k_{hM}, k_{vL}/k_{vM} and h_L/h_M used to show the effect of changing k_{hL}/k_{hM}, k_{vL}/k_{vM} and h_L/h_M on the amount of bypassed reserves left in the laminated layer. Each Cases 1, 3 and 5 are the same and used for comparison in Figures 2.5 and 2.6. Cases 2, 4 and 6 each increase one of the ratios (highlighted) and are used in Figures 2.5 and 2.6 to show the effect of increasing these ratios on the amount of bypassed reserves.

Horizontal Permeability Ratio (k_{hL}/k_{hM})

Reserves are bypassed in the laminated layer when both layers are perforated in two-layer reservoirs with crossflow because the horizontal gas fluxes are higher in the massive layer than in the laminated layer. The difference in horizontal gas flux between the layers is caused by the difference in horizontal permeabilities between the layers (Fig 2.3). An increase in the permeability of the laminated layer relative to the massive layer (k_{hL}/k_{hM}) results in increased horizontal gas fluxes in the laminated layer (Fig 2.4A Case 1 to Case 2). Increased horizontal gas fluxes in the laminated layer decreases the difference between the laminated layer horizontal gas fluxes and the massive layer horizontal gas fluxes in Case 2. A decreased gas flux difference between the laminated and massive layers in Case 2 compared to Case 1 (Fig 2.4A) results in the GWC of the massive layer moving slower with respect to the GWC of the laminated layer. A slower moving GWC in the massive layer allows more reserves to be produced from the laminated layer before water reaches the wellbore in the massive layer.

Vertical Permeability Ratio (k_{vL}/k_{vM})

Modifying k_{vL}/k_{vM} changes the amount of reserves that crossflow from the laminated layer into the massive layer. Increasing k_{vL}/k_{vM} (Fig. 2.4B, Case 3 vs. 4) increases the vertical gas fluxes of from the laminated layer to the massive layer, adding to the reserves in the massive layer. If there are more reserves in the massive layer and the same amount of gas is being produced from the massive layer because the well capacity has not changed (k_{hL} h_L, k_{hM} h_M) then it is going to take longer for the massive layer GWC to reach the wellbore. The slowing of the massive layer GWC encroachment in Case 4

compared to Case 3 allows more reserves to be produced from the laminated layer before water reaches the wellbore in the massive layer; the amount of bypassed reserves decreases.

Net Thickness Ratio (h_L/h_M)

Recovery is decreased if h_L/h_M is increased (Fig. 2.5 Case 5 vs. 6). If h_M is equal in Cases 5 and 6 then to increase h_L/h_M between Case 5 and Case 6, h_L must increase. Increasing h_L between Case 5 and Case 6 increases the volume of reserves in the laminated layer (Fig. 2.5). The increased thickness of the laminated layer in Case 5 compared to Case 6 increases the wellbore flow capacity of the laminated layer (k_{hL} h_L). The amount of bypassed reserves in the laminated layer in Case 6 compared to Case 5 depends on if the increased well capacity makes it possible to produce the increased volume of reserves in the laminated layer of Case 6 compared to Case 5 before the GWC in the massive layer reaches the wellbore in each of the cases. Simulations show that the increase in well capacity between Case 5 and Case 6 does not compensate for the increased volume in Case 5 compared to Case 6; recovery decreases between Case 5 and Case 6.

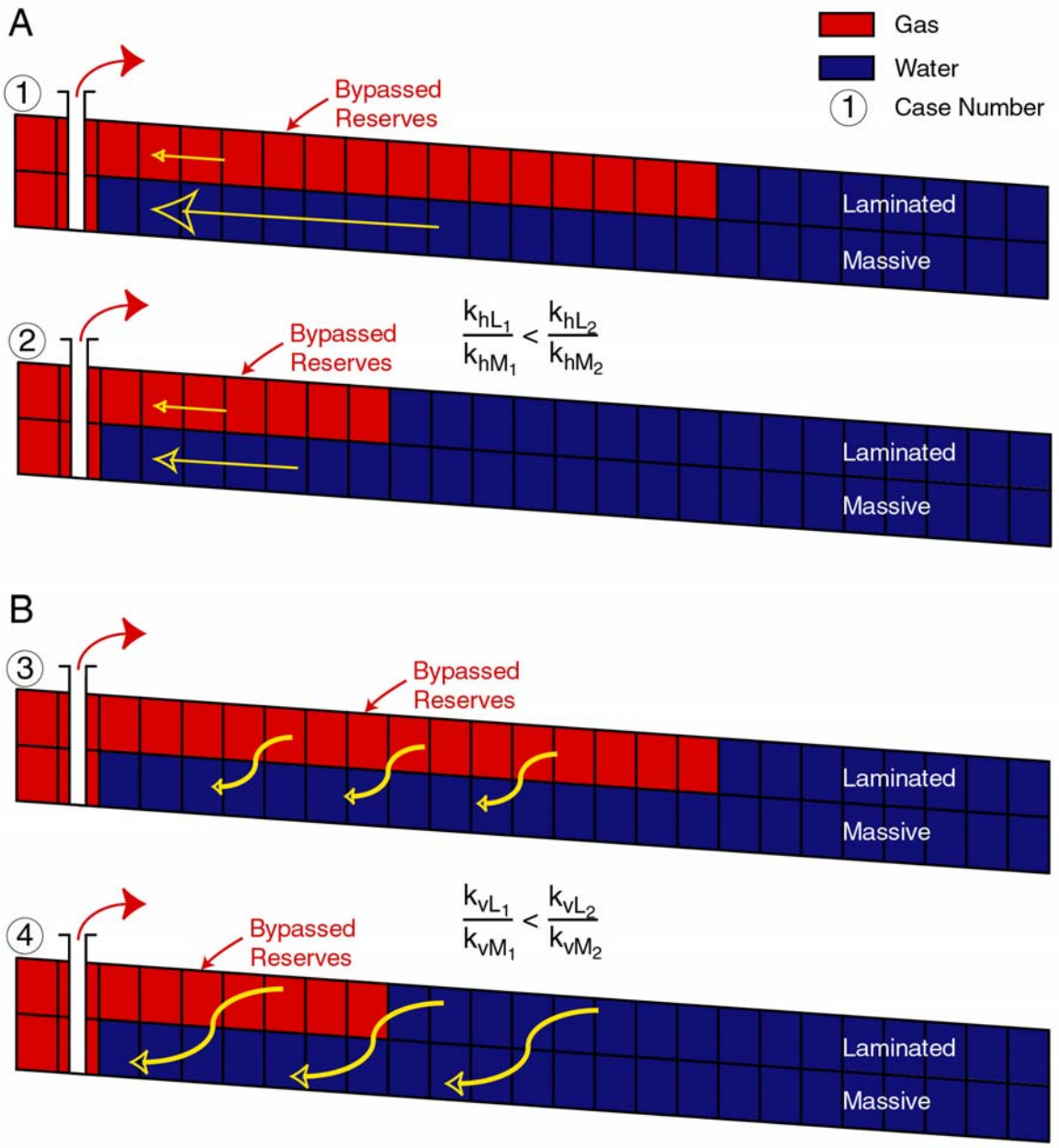

Figure 2.4: Qualitative Cross-section showing the effects of increasing (A) k_{hL}/k_{hM} and (B) k_{vL}/k_{vM} on the amount of bypassed reserves in the laminated layer. Cases 1 and 3 have the same k_{hL}/k_{hM}, k_{vL}/k_{vM}, and h_L/h_M. Cases 2 and 4 increase k_{hL}/k_{hM} and k_{vL}/k_{vM}, respectively, while the other two ratios are kept constant. Yellow arrows are qualitative gas flux arrows that show how changing k_{hL}/k_{hM} (A) effects the horizontal gas flux in each layer and how changing k_{vL}/k_{vM} (B) effects the vertical gas flux between layers. Case numbers used in the text refer to case numbers for the cross-sections of this figure and Figure 2.5.

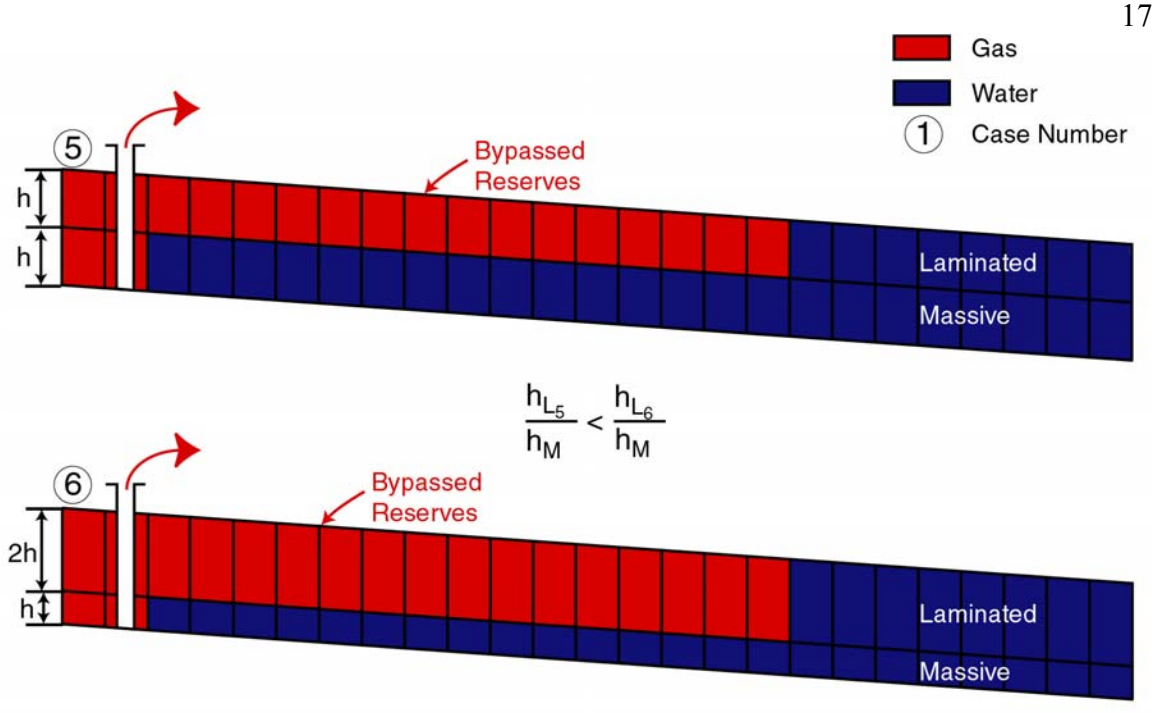

Figure 2.5: Qualitative cross-section showing the effect of increasing h_L/h_M on the amount of bypassed reserves in the laminated layer. k_{hL}/k_{hM} and k_{vL}/k_{vM} are constant between Case 5 and Case 6. h_L is larger in Case 6 than in Case 5. Case numbers used in the text refer to case numbers for the cross-sections of this figure and Figure 2.4.

Recovery Optimization

An obvious solution to the problem of bypassed reserves is to only produce from the laminated layer; this approach is considered here. The simple system with k_{vL}/k_{vM} equal to 0.0001, k_{hL}/k_{hM} equal to 0.42, and h_L/h_M equal to 2.0 (Table 2.1) is used to demonstrate that perforating only the laminated layer can effectively produce the bypassed reserves. This is the same simple model as in the Flow Characteristics section with only the laminated layer is perforated.

When producing from both layers of two-layer reservoirs with crossflow, lower pressures develop in the laminated layer compared to the massive layer (Fig. 2.6A). This pressure difference allows massive layer reserves to flow vertically into the laminated

layer, and then flow into the wellbore (Fig. 2.6B). The massive layer has lower gas potential gradients than the horizontal gas gradients laminated layer (Fig. 2.6A) and a higher horizontal permeability than the horizontal permeability of the laminated layer (k_{hL}/k_{hM} = 0.42, Table 2.1). This leads to similar horizontal gas fluxes in both the laminated and massive layers. As a result, the GWC of the laminated layer moves at a similar rate to the GWC of the massive layer (Fig 2.6C). Because the GWC of both layers are moving equally, the reserves in the massive layer can flow into the laminated layer before the GWC of the laminated layer reaches the wellbore (Fig. 2.7).

Simulations are performed using the simple system to investigate what effect changing k_{hL}/k_{hM}, k_{vL}/k_{vM}, h_L/h_M and perforation strategy has on hydrocarbon recovery. For each combination of k_{hL}/k_{hM}, k_{vL}/k_{vM} and h_L/h_M, a simulation exercise is performed with only the laminated layer perforated (Table B-1). The same exercise is repeated with both layers of the reservoir perforated (Table B-1). The results of these simulations are compared to determine which production strategy recovers more hydrocarbons.

Recovery Optimization simulations simulated reservoir production for 18 years. Simulations performed with perforations in both layers depleted the reservoir in less than five years. Some simulations performed with only the laminated layer perforated took more than 18 years but were cut off at 18 years because by this point the better perforation strategy was easily discernable.

It is worth noting that the optimization protocol only considers changes in the input values for the ratios k_{hL}/k_{hM}, k_{vL}/k_{vM} and h_L/h_M (Table 2.1). It does not consider changes in any other simulation input values such as water volume, changes in reservoir structure, capillary pressure curves, relative permeability curves, compaction models, or porosity.

Initial simulations showed that these variables can have a significant effect on the results of the optimization protocol.

The optimization protocol also only considers implementing the two different perforation strategies at the onset of production. No studies were performed, using the simple model, that consider changing perforation strategies after the onset of production.

Methods of Comparing Production Strategies

We compare simulations by using recovery difference (*RD*):

$$RD = RD_B - RD_{OL}, \qquad 2.1$$

where RD_B is the recovery when both layers of the reservoir are perforated, and RD_{OL} is the recovery with only the laminated layer perforated. *RD* values that are zero signify that it is equally beneficial to perforate both layers and to only perforate the laminated layer. Negative *RD* values indicate that perforating only the laminated layer improves the recovery from the reservoirs; positive *RD* values represent reservoirs that benefit from perforating both layers.

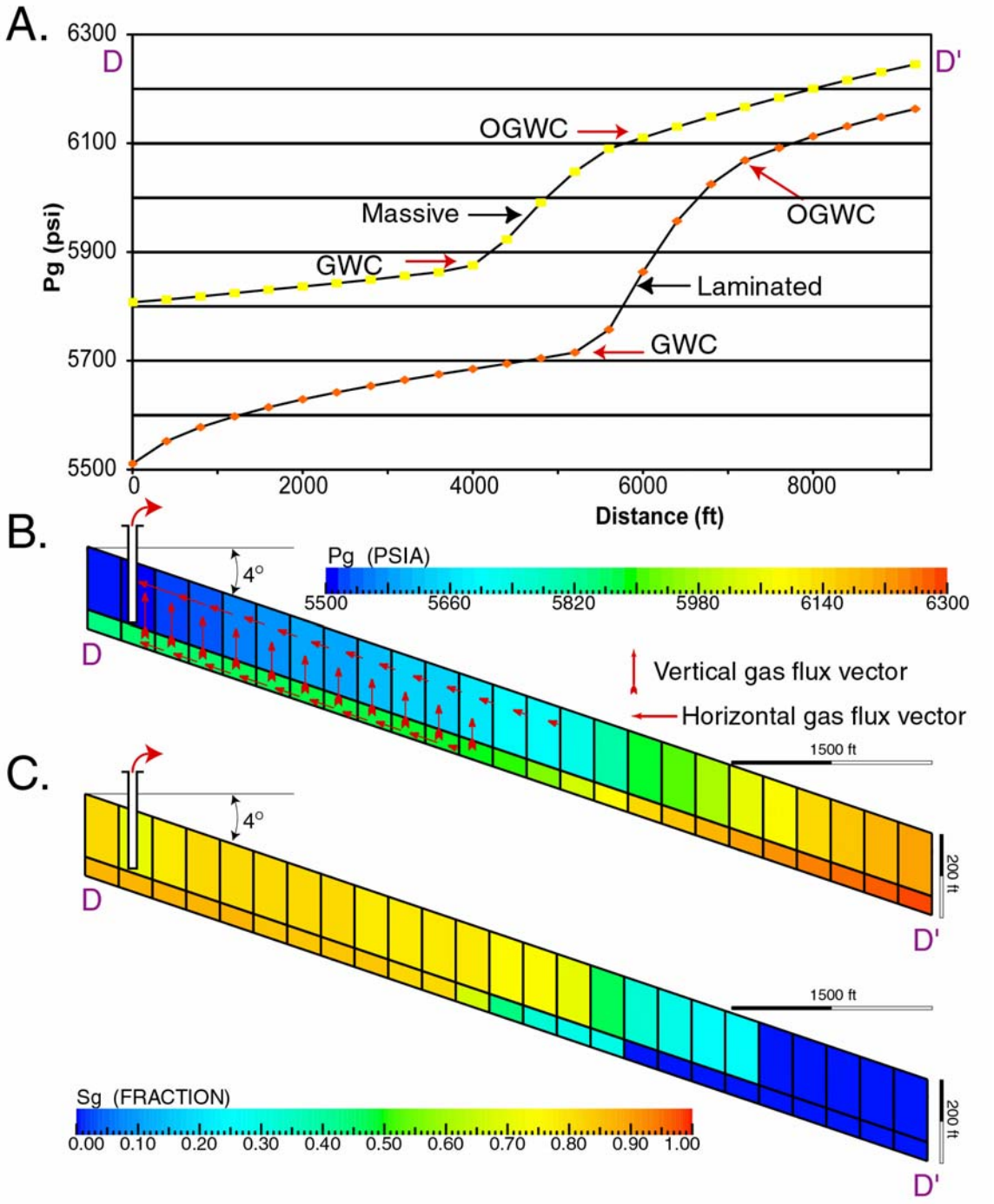

Figure 2.6: (A) Grid block gas pressure (Pg) (547 days) versus distance away for the wellbore for cross-section D-D' (Fig. 2.1). (B) Cross-section D-D' (Fig. 2.1) of Pg after 547 days of simulation. Vertical and horizontal gas flux vectors are shown. The magnitude of a horizontal gas flux vector is 5000 times greater then that of a vertical gas flux vector of the same length. (C) Cross-section D-D' (Fig. 2.1) shows gas saturation (Sg) after 547 days. After 547 days of production the reservoir has produced 136 BCF. These results are taken from simple system 130 (red, Table B-1)

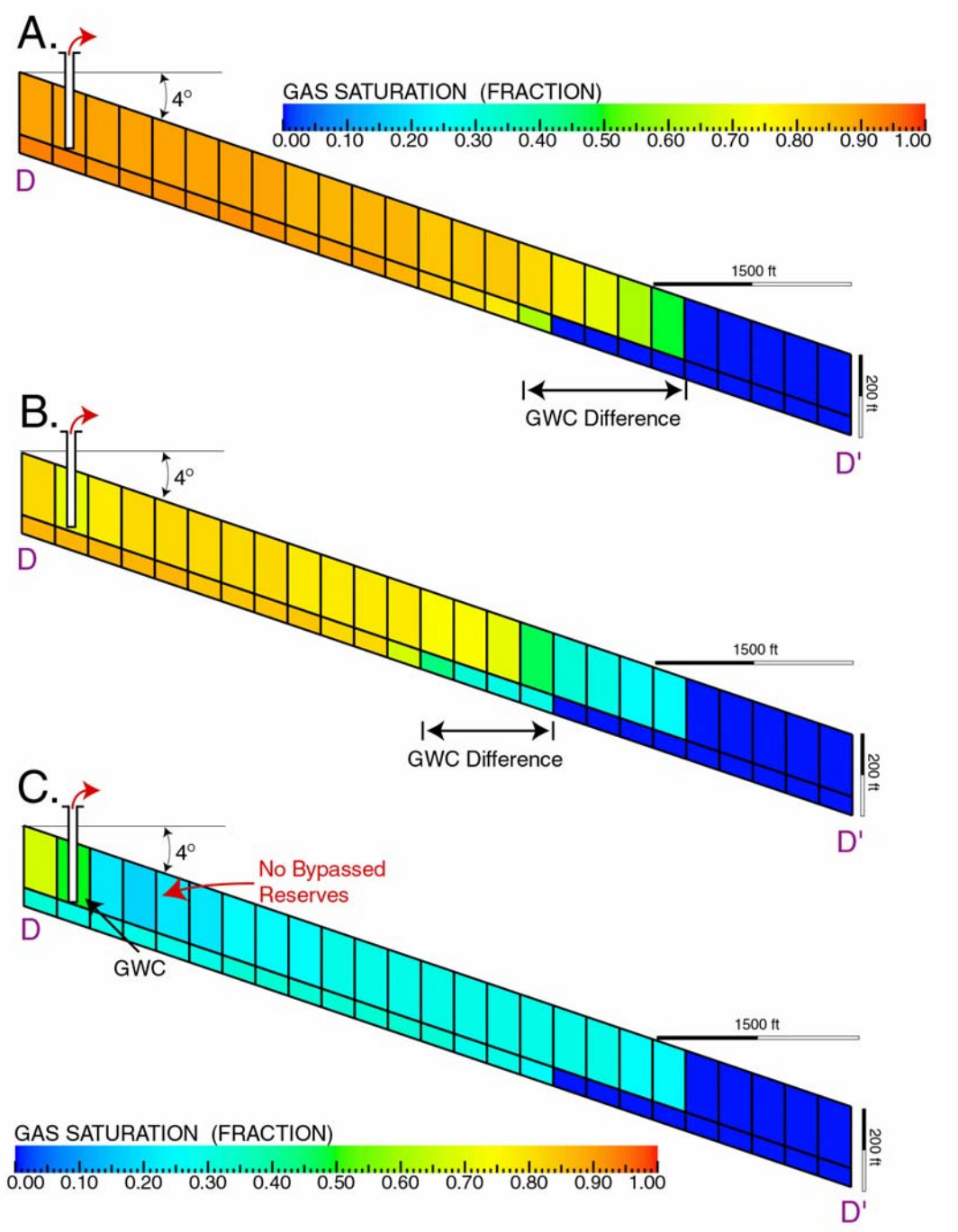

Figure 2.7: Cross-sections D-D' (Fig. 2.1) showing gas saturation through time, (A) initial, (B) 547 days after production began and (C) final (1641 days) for simple system 130 (red, Table B-1). The difference in GWC between the laminated and massive layer is highlighted initially and at 547 days. The final GWC is at the wellbore in the laminated layer and the massive layer is totally depleted. Figure 2.6 contains a plot and cross-sections of additional fluid properties for the same cross-section at 547 days (B).

Optimization Protocol

Values of *RD* are calculated for simulations performed with various combinations of k_{hL}/k_{hM}, k_{vL}/k_{vM}, and h_L/h_M (Table B-1). For each value of k_{vL}/k_{vM} tested, a two-dimensional contour plot of *RD* values is created with k_{hL}/k_{hM} and h_L/h_M as the *x* and *y* axis (Fig 2.8). A series of plots (Figs. 2.8-2.12) illustrates the results for the range of k_{vL}/k_{vM} values tested (Table B-1). This collection of plots is considered the optimization protocol and suggests if it is better to perforate only the laminated layer or to perforate both layers of a two-layer reservoir with crossflow based on k_{hL}/k_{hM}, k_{vL}/k_{vM}, and h_L/h_M.

The contour plot of the optimization protocol where k_{vL}/k_{vM} equals 0.0001 and a range of values for k_{hL}/k_{hM} and h_L/h_M is used to highlight specific areas of interest (Fig. 2.8: Table B-1). The greatest benefit to perforating only the laminated layer is when h_L/h_M equals 2.0 and k_{hL}/k_{hM} equals 1.3 (orange circle, Fig. 2.8) For reservoirs with h_L/h_M ratios less than approximately 0.5 (red zone, Fig. 2.8) it is detrimental to perforate only the laminated portion of the reservoir. This is also true for reservoirs where k_{hL}/k_{hM} is less than approximately 0.1 (green zone, Fig. 2.8). As h_L/h_M increases (blue arrow, Fig. 2.8) it becomes more beneficial to produce from only the laminated layer. As k_{hL}/k_{hM} increases it becomes less beneficial to perforate only the laminated layer (purple arrow, Fig 2.8).

Simple systems that have a lot of reserves bypassed when both layers are perforated show the greatest increase in recovery when only the laminated layer is perforated (orange circle, Fig. 2.8). When k_{hL}/k_{hM} equals 1.3 and h_L/h_M equals 2.0, h_L is thick compared to h_M and k_{hL} is low compared to k_{hM}. These conditions result in a large amount of bypassed reserves that are produced when only the laminated layer is perforated.

The dependence of improving recovery by only perforating the laminated layer on the amount of bypassed reserves is also illustrated by looking at how the benefit of producing from the laminated layer increases as h_L/h_M increases (blue arrow, Fig.2.8). As h_L/h_M increases the amount of bypassed reserves increases and as a result the benefit of only perforating the laminated layer increases. The same reasoning can be used to explain why the benefit of producing from only the laminated layer decreases as k_{hL}/k_{hM} increases. If both layers of the reservoir are perforated the amount of bypassed reserves decreases as k_{hL}/k_{hM} increases. There just aren't as many bypassed reserves to be produced so the benefit of perforating only the laminated layer decreases.

The large positive *RD* values when k_{hL}/k_{hM} is less than approximately 0.8 (green area, Fig. 2.8) and h_L/h_M is less than approximately 0.5 (red area, Fig. 2.8) are indicative of when the well capacity of only perforating the laminated layer is so low that the reservoir become pressure deplete before all of the reserves can be produced. Additionally, when k_{hL}/k_{hM} is less than approximately 0.25 and k_{hL}/k_{hM} is less than approximately 0.5 (Fig. 2.8) the 18 year simulation time-limit begins to decrease the amount of fluids produced when only the laminated layer is perforated. This accentuates the benefit of perforating both layers.

The main difference seen as k_{vL}/k_{vM} increases is that the magnitude of the negative *RD* values decreases (Fig 2.8-2.12). The change in magnitude as k_{vL}/k_{vM} increases is again dependant on the amount of reserves bypassed when both layers of a specific reservoir model are perforated. Since the amount of reserves bypassed when both layers of the reservoir are perforated increases as k_{vL}/k_{vM} decreases the benefit of producing from only the laminated layer of reservoirs increases as k_{vL}/k_{vM} decreases.

The influence of crossflow on production strategy can also be shown by looking specifically at how the zero contour line changes as k_{vL}/k_{vM} increases. As k_{vL}/k_{vM} decreases the portion of the zero *RD* contour line that is greater than 0.3 k_{hL}/k_{hM} moves towards higher values of k_{hL}/k_{hM} until k_{vL}/k_{vM} equals 0.0004. Then it begins to move back towards smaller values of k_{hL}/k_{hM} (Figure 2.13) as k_{vL}/k_{vM} decreases. Originally, the change in position of the zero *RD* contour line as k_{vL}/k_{vM} decreases is due to the increase in bypassed reserves, when both layers are perforated, as k_{vL}/k_{vM} decreases. Once k_{vL}/k_{vM} reaches 0.0004 the decreasing k_v begins to affect the crossflow of reserves from the massive layer into the laminated layer when only the laminated layer is perforated. The zero *RD* contour line shift for values of k_{vL}/k_{vM} greater than 0.0004 is towards higher values of k_{hL}/k_{hM} because larger amounts of bypassed reserves in the laminated layer, when both layers perforated, are required to over come the reduction in reserves that crossflow form the massive layer into the laminated layer when only the laminated layer is perforated.

The optimization protocol suggests that only the laminated layer of a two-layer reservoir with crossflow should be perforated when $0.00005 \leq k_{vL}/k_{vM} \leq 0.0008$, $0.1 \leq k_{hL}/k_{hM} \leq 0.65$, and $h_L/h_M \geq 0.75$. The protocol also showcases the effect changing k_{hL}/k_{hM}, k_{vL}/k_{vM}, and h_L/h_M has on the amount of reserves bypassed in the laminated layer when both layers of two-layer reservoirs with crossflow are perforated.

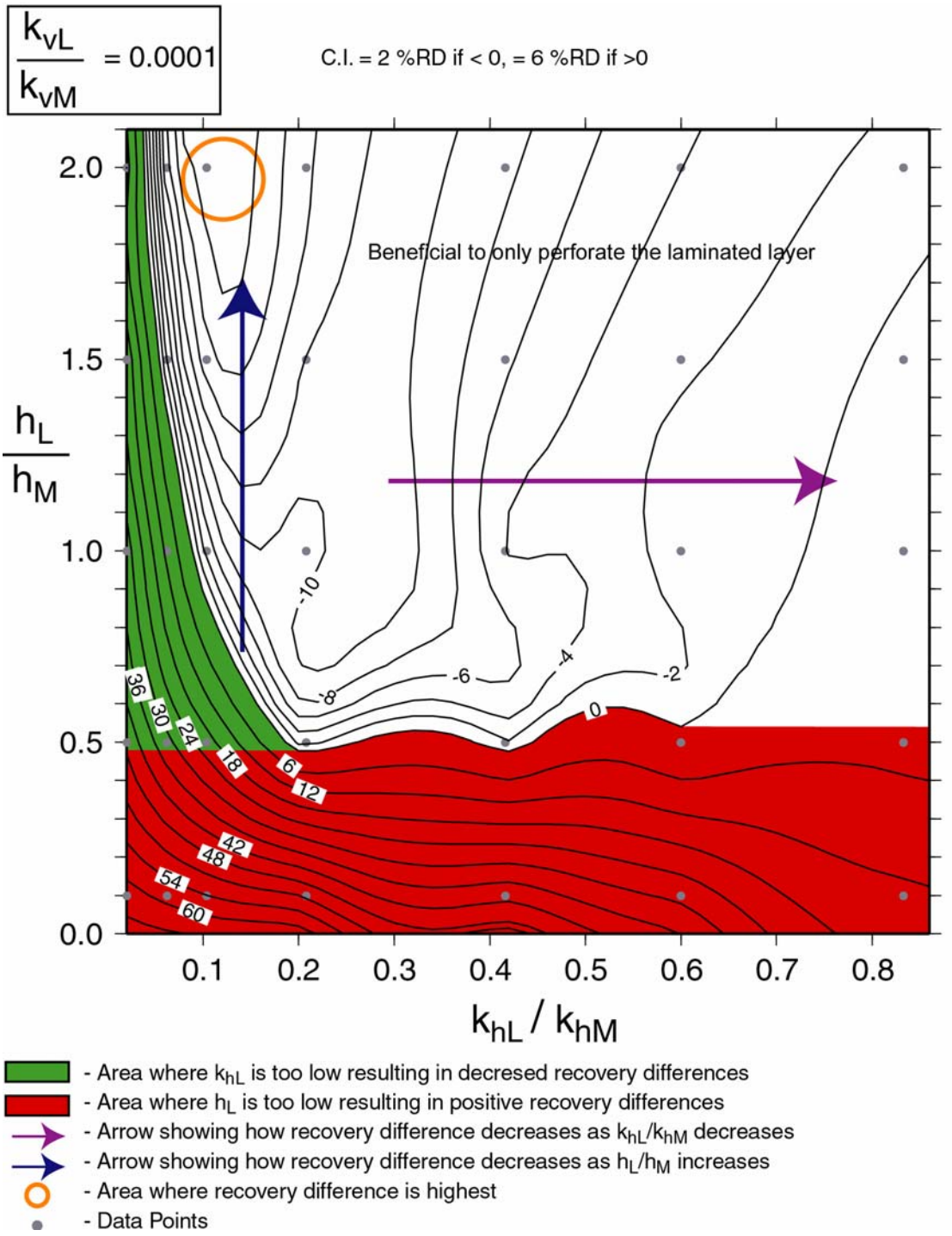

Figure 2.8: Contour plot showing the recovery difference (*RD*, Eq. 2.2) between perforating both layers and only perforating the laminated layer for k_{vL}/k_{vM} of 0.0001 and various values of k_{hL}/k_{hM} and h_L/h_M (Table B-1). The zero contour on this plot shows simulations where it is equally beneficial to perforate only the laminated layer or both layers. Positive contours are simulations where perforating both layers is better then perforating only the laminated layer and negative contours are when it is beneficial to only perforate the laminated layer. Figures 2.8 to 2.12 are considered the optimization protocol.

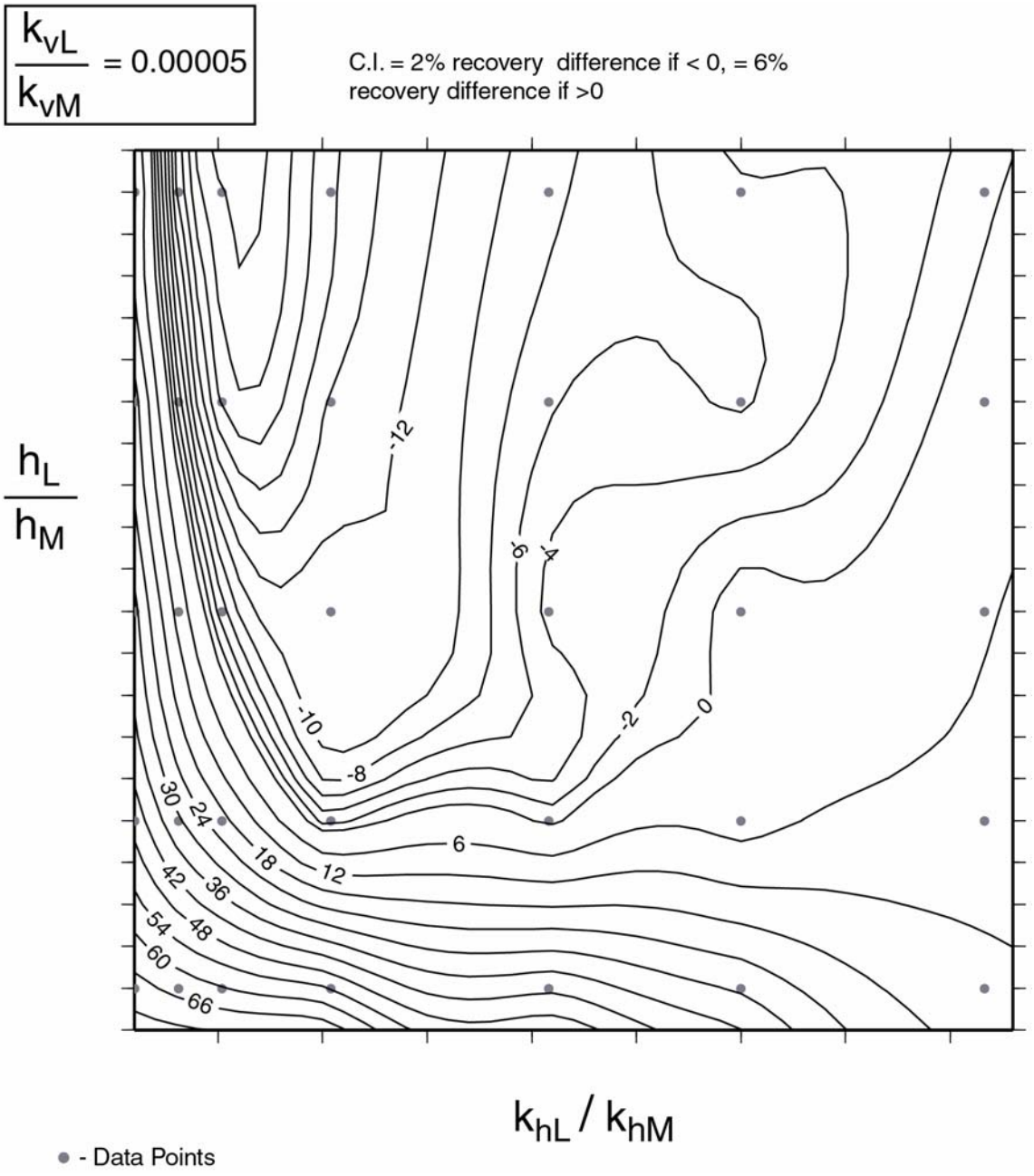

Figure 2.9: Contour plot showing the recovery difference between perforating both layers and only perforating the laminated layer for k_{vL}/k_{vM} of 0.00005 and various values of k_{hL}/k_{hM} and h_L/h_M (Table B-1).

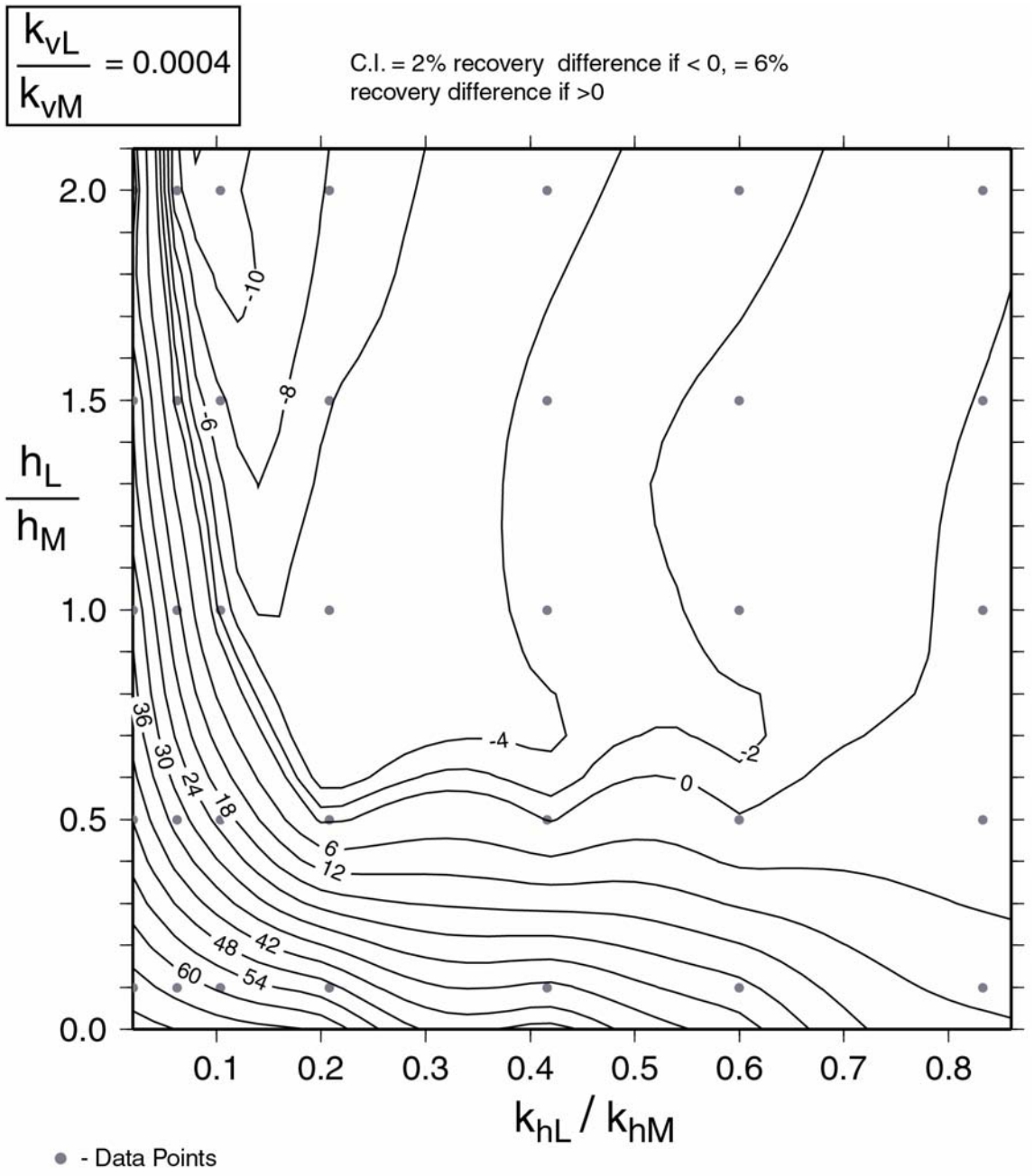

Figure 2.10: Contour plot showing recovery difference between perforating both layers and only perforating the laminated layer for k_{vL}/k_{vM} of 0.0004 and various values of k_{hL}/k_{hM} and h_L/h_M (Table B-1).

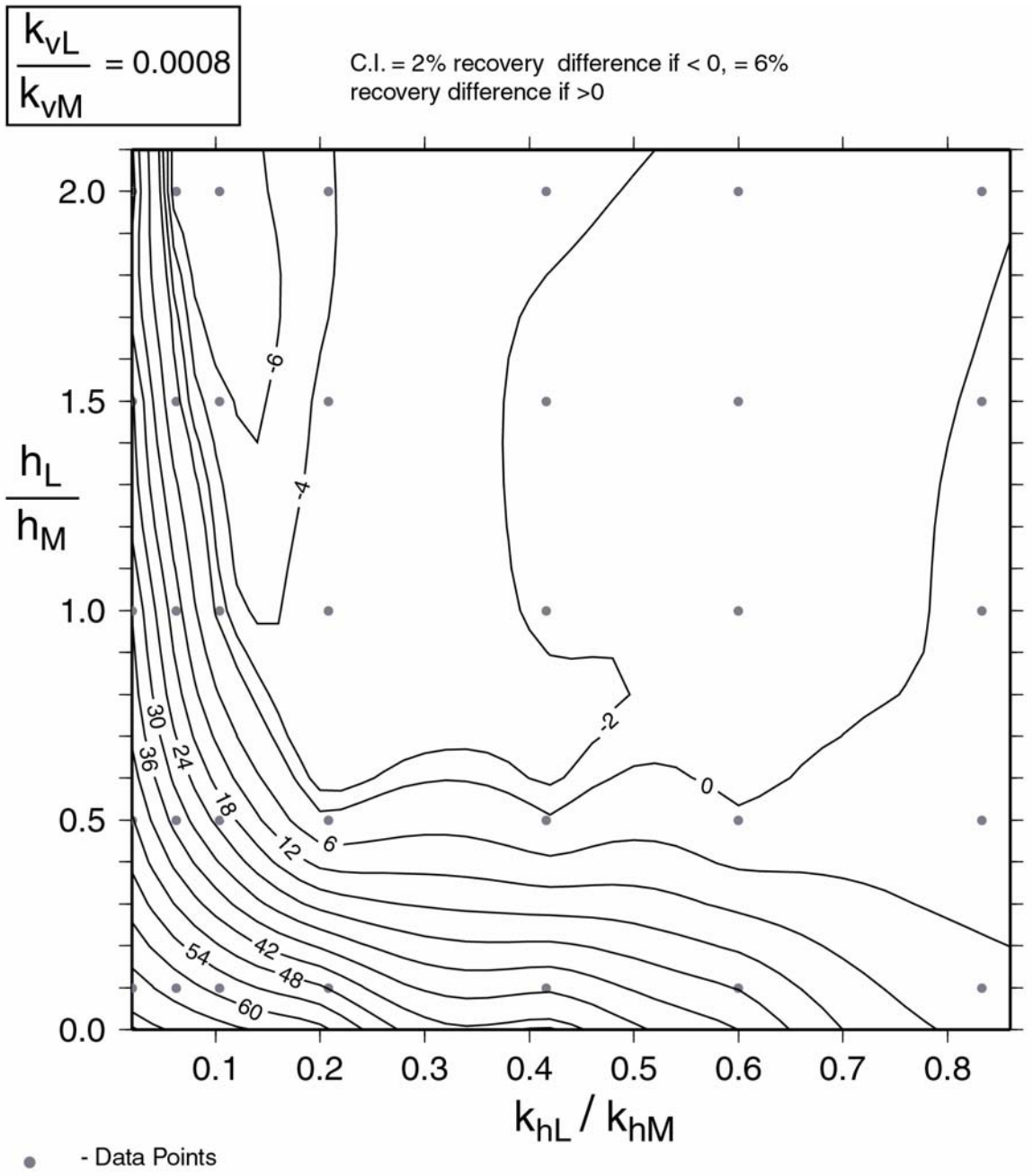

Figure 2.11: Contour plot showing the recovery difference between perforating both layers and only perforating the laminated layer for k_{vL}/k_{vM} of 0.0008 and various values of k_{hL}/k_{hM} and h_L/h_M (Table B-1).

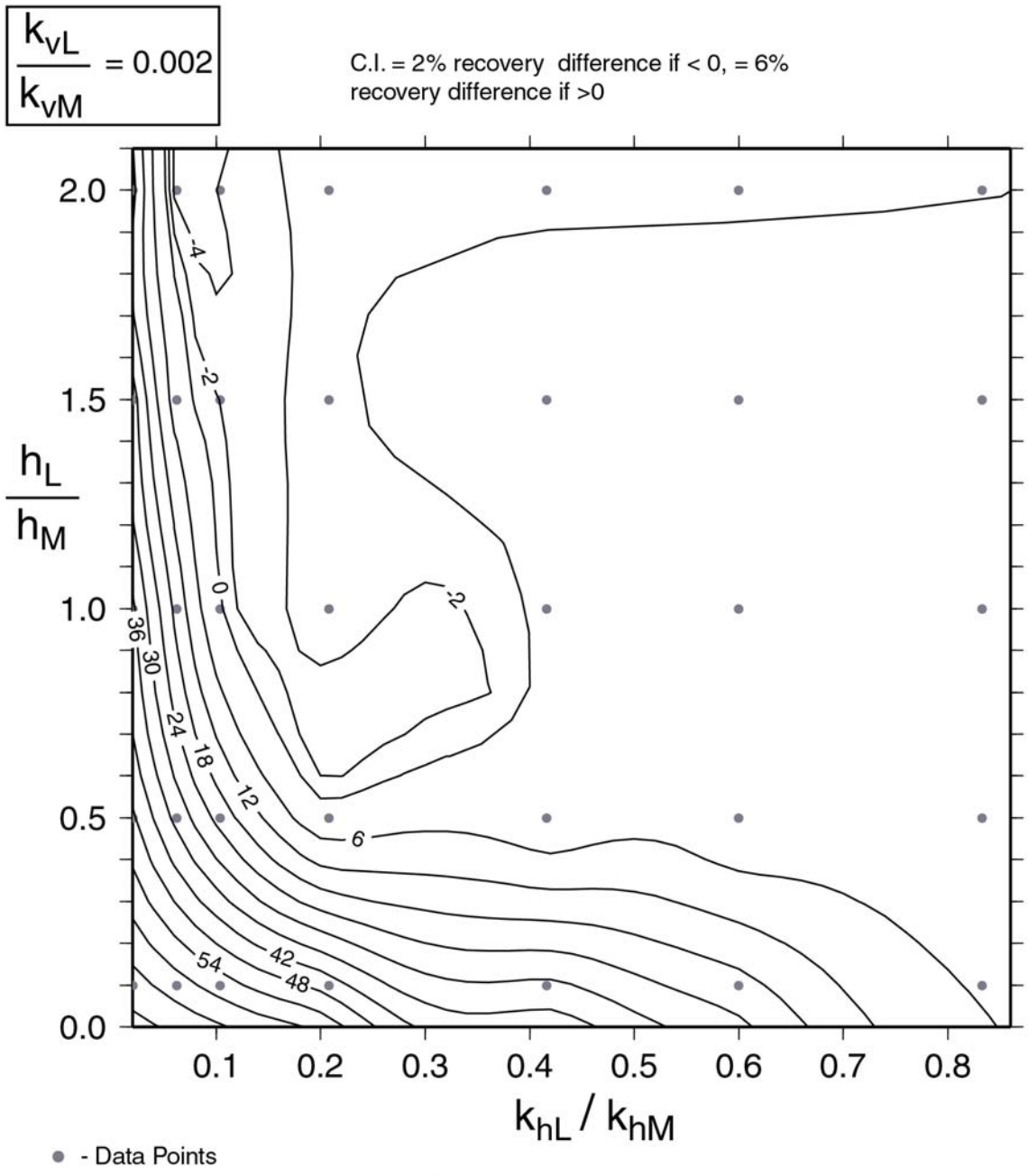

Figure 2.12: Contour plot showing the recovery difference between perforating both layers and only perforating the laminated layer for k_{vL}/k_{vM} of 0.002 and various values of k_{hL}/k_{hM} and h_L/h_M (Table B-1).

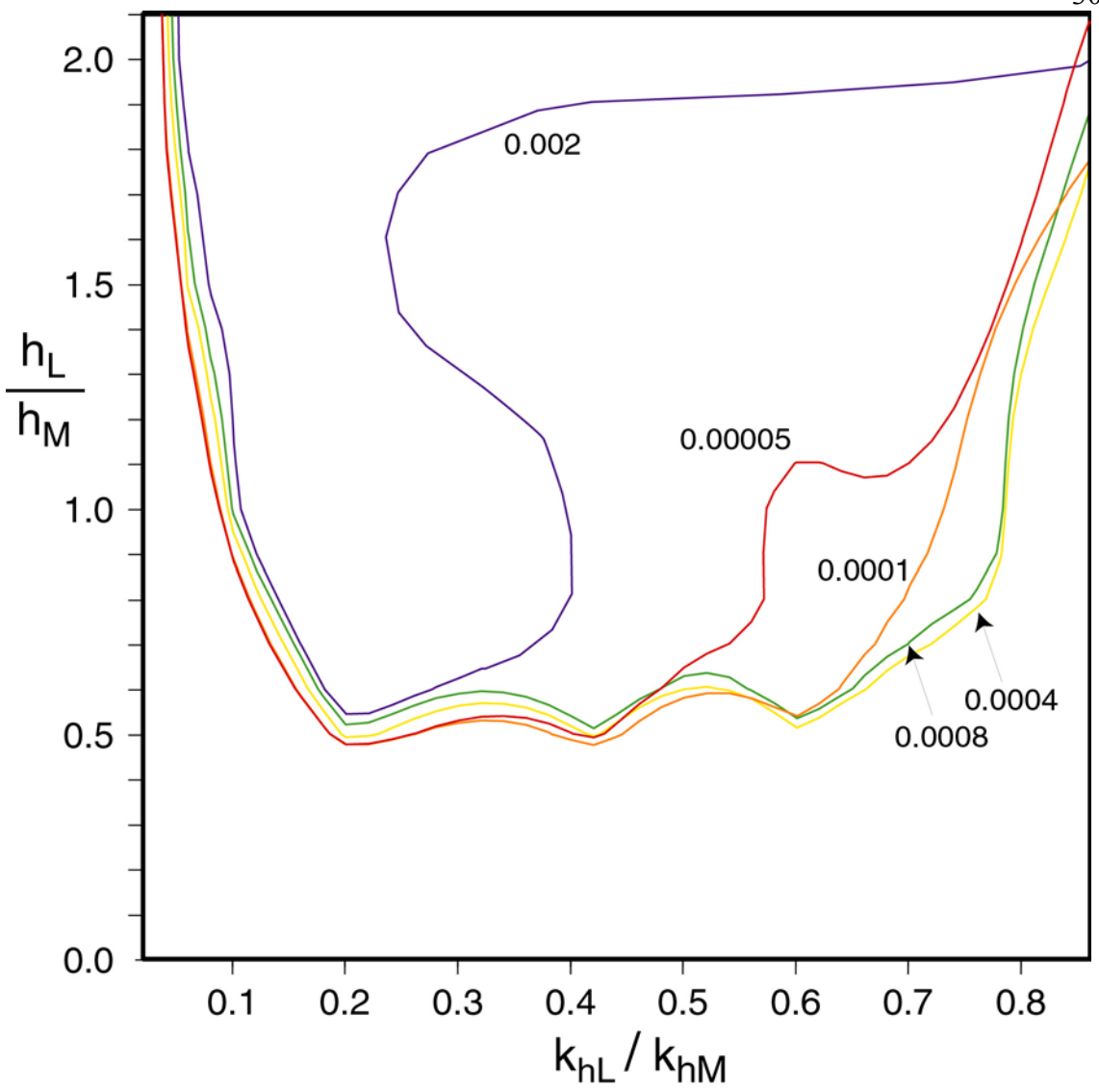

Figure 2.13: Change in zero *RD* contour line as k_{vL}/k_{vM} increases. Each zero *RD* contour line is labeled based on the value of k_{vL}/k_{vM} from the plot that it was extracted from (Figs. 2.8-2.12). A *RD* contour line of zero means that it is equally beneficial to perforate the laminated layer and to perforate both layers. Above the zero *RD* contour line is the region where *RD* values are negative and bellow the zero *RD* line are the values of *RD* that are positive.

Inclusion of the Time Value of Money

The time value of money considers the economic effects of having reduced well rates over a longer period of time when only the laminated layer is perforated compared to having higher well rates for a shorter period of time when both layers of the formation are perforated. In order to consider the economic effects of the different rates between production strategies, recovery present value (*RPV*) is calculated for each simulation. The equation for *RPV* is

$$RPV = \sum_{t=1}^{n} \frac{Q\%R}{(1+r)^t}, \qquad 2.2$$

where *RPV* is the recovery present value, *n* is the total number of quarterly time intervals since initial production, *Q%R* is the percent recovery in a specific quarter year increment, *r* is the quarterly discount rate calculated from an annual discount rate, and *t* is the number of quarter year increments between initial production and the *Q%R* being discounted.

A method simliar to that used to compare perforation strategies based on total recovery from the reservoir (*RD*) can be used consider the economic implications of the two different perforation strategies. This is accomplished by computing the difference between an *RPV* for a simulation with only the laminated layer perforated (RPV_{OL}) and an *RPV* for a simulation with both layers perforated (RPV_B):

$$DRPV = RPV_B - RPV_{OL} \qquad 2.3$$

where *DRPV* is the difference in *RPV* between the two perforation strategies. For the *DRPV* results shown in this study, an annual discount rate of 7% was used for *RPV* calculations. Positive *DRPV*s imply that either more hydrocarbons are recovered with

both layers perforated or that the well capacity when only the laminated layer is perforated is too low to be economically viable; negative *DRPV*s indicate that it is better to perforate only the laminated layer.

Lower well rates due to only perforating the laminated layer increases the amount of time it takes to produce all of the reserves from the reservoir. When the time value of money is considered, the further into the future reserves are produced the more they are discounted. Therefore, in order to have a negative *DRPV*, not only do more hydrocarbons have to be recovered when only the laminated layer is perforated but the reserves also need to be produced in a timely manner.

Including economics reduces how influential the amount of bypassed reserves is on the perforation strategy. For contour plots made for the same simulations, the area of the most negative *RD* values does not correspond to the area of the most negative *DRPV* values (Fig. 2.14). The economics calculations (*DRPV*) do not support only perforating the laminated layer when k_{hL}/k_{hM} is less than approximately 0.15 and h_L/h_M is less than approximately 1.0 (Fig 2.14B). Even though the amount of bypassed reserves increases as k_{hL}/k_{hM} decreases, the time that is takes to produce those reserves increases due to lower k_h. In addition, as h_L/h_M decreases the time it takes to produce the reserves from the reservoir increases due to lower h_L.

The overall decrease in the magnitude of the negative *DRPV* values compared to the negative *RD* values is because the *DRPV* values are discounted and the *RD* values are not. The discounting reduces the *RPV* values that are differenced to determine the *DRPV* and since both RPV_{OL} and RPV_B are less then the total field recovery of each simulation the magnitude of the *DRPV* value is also going to be less. This is accentuated in the

simulations that are beneficial to perforate only the laminated layer because these reservoirs were fully produced before the 18 year time limit. The difference between *RD* and *DRPV* values is less when k_{hL}/k_{hM} is less than approximately 0.05 and h_L/h_M is less than approximately 0.25 because the reservoirs under these conditions are not fully depleted after 18 years and cutting off production is effectively the same as discounting the reserves using the economic calculations.

The effect of increasing k_{vL}/k_{vM} on the *DRPV* contour plots is best illustrated by observing the change in the zero *DRPV* contour line as k_{vL}/k_{vM} increases (Fig. 2.15). The reduction of well rates due to only perforating the laminated layer becomes more pronounced as k_{vL}/k_{vM} increases. In the economic calculations (*DRPV*), the increased recovery due to only perforating the laminated layer is not able to compensate for the additional time that it takes to produce the reserves.

When economics are considered, the benefit of only perforating the laminated layer of two-layer reservoirs with crossflow is reduced because the rates wells can produce at is reduced. The effect lower well rates has on how beneficial it is to perforate the laminated layer is dependent on the economics model used, specifically, in this case it depends on the discount rate (r) used to calculate *RPV*.

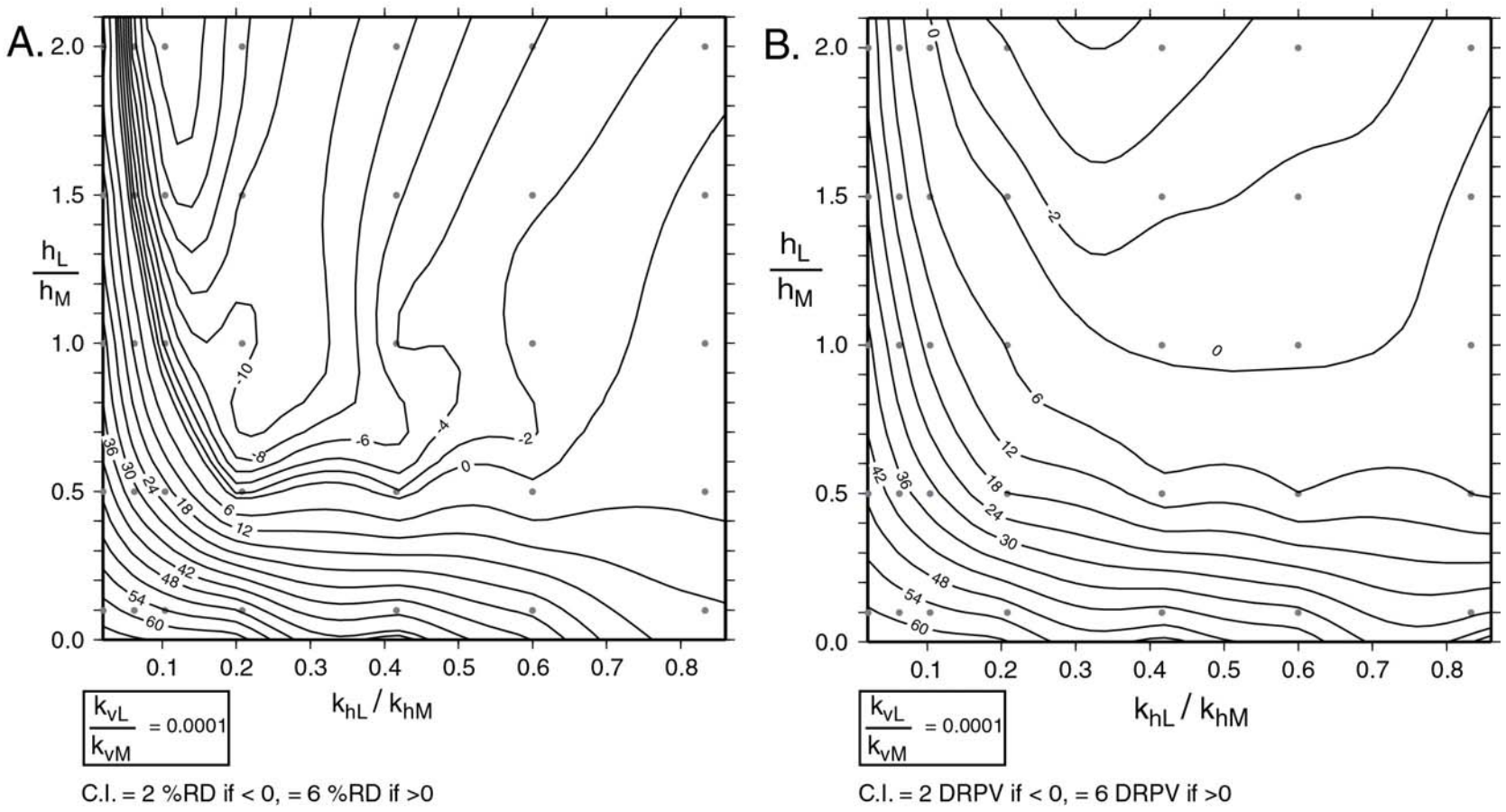

Figure 2.14: (A) *RD* contour plot for k_{vL}/k_{vM} equal to 0.0001 and various values of h_L/h_M and k_{hL}/k_{hM} (Table B-1 Simulation 106-130). (B) *DRPV* (Eq. 2.1) contour plot for same simulation as (A) but the recoveries are discounted based on a 7% discount rate used for *RPV* calculations (Eq. 2.2). Contour plot (B) shows the results of performing the economic calculations (*RPV* and *DRPV)* on the simulation results used to produce contour plot (A).

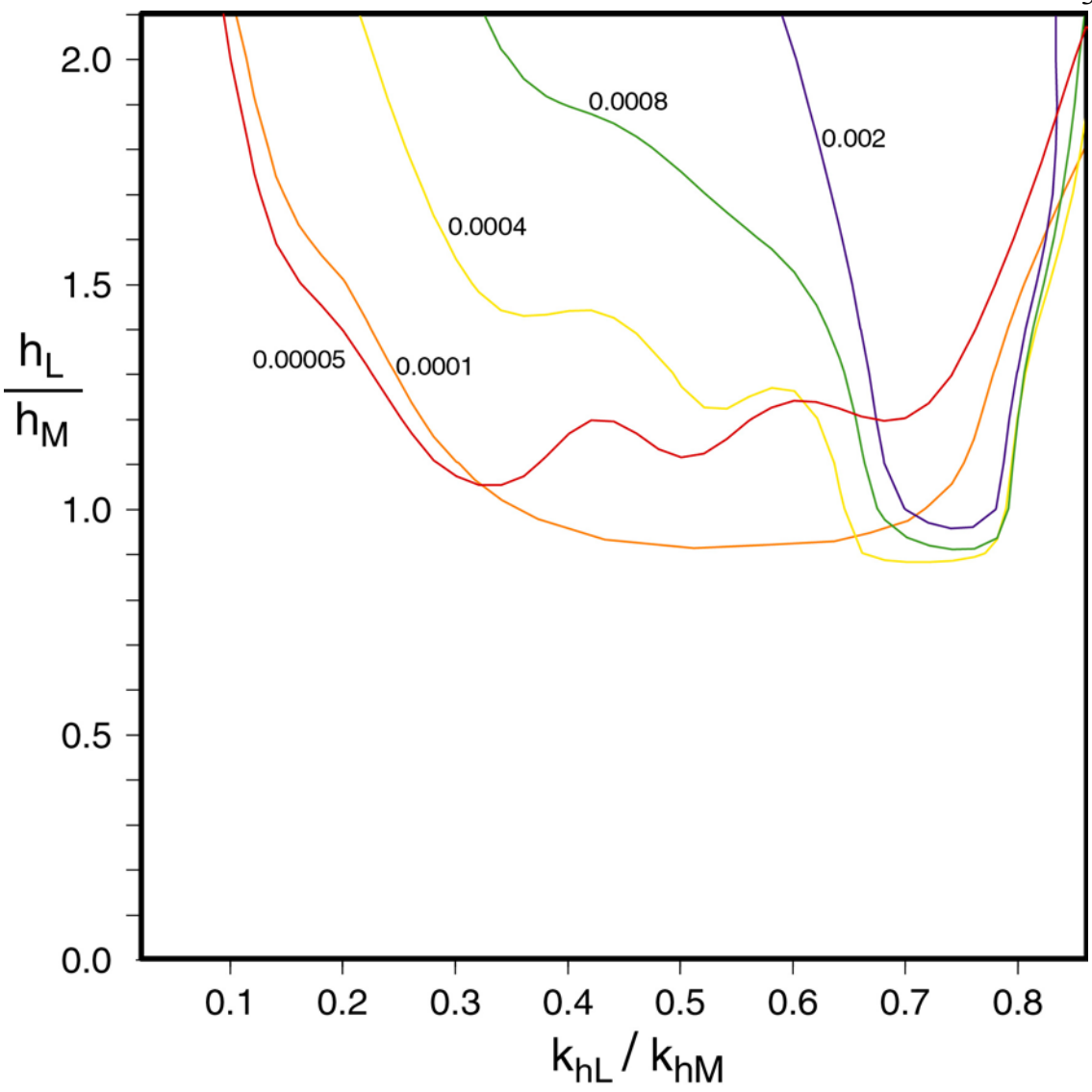

Figure 2.15: Change in zero *DRPV* contour line as k_{vL}/k_{vM} increases. Each zero *DRPV* contour line is labeled based on the value of k_{vL}/k_{vM} it is associated with. A *RD* contour line of zero means that it is equally beneficial to perforate the laminated layer and to perforate both layers. Above the zero *DRPV* contour line is the region where *DRPV* values are negative and bellow the zero *DRPV* line are the values of *DRPV* that are positive.

Conclusions

It is possible to predict if producing from only the laminated layer of two-layer reservoirs with crossflow will increase recovery from the field. Recovery is increased by only perforating the laminated layer of reservoirs where $0.00005 \leq k_{vL}/k_{vM} \leq 0.0008$, $0.1 \leq k_{hL}/k_{hM} \leq 0.65$, and $h_L/h_M \geq 0.75$. However, only perforating the laminated layer of two-layer reservoirs with crossflow reduces the well capacity and therefore the rates at which reserves can be produced from the reservoir. This has implications on the economic viability of producing from only the laminated layer of two-layer reservoirs with crossflow. These effects can be evaluated by using the *DRPV* calculation.

References

Bayat, M. G., and D. H. Tehrani, 1985, The Thistle Field - Analysis of its past performance and optimization of its future development: Offshore Europe 85 Conference.

Bilozir, D. E., and P. M. Frydl, 1989, Reservoir description and performance analysis of a mature miscible flood in Rainbow Field, Canada: 64th Annual Technical Conference and Exhibition of the Society of Petroleum Engineers.

Lerch, C. S., K. W. Bramlett, W. H. Butler, J. N. Scales, T. B. Stroud, and C. A. Glandt, 1996, Integrated 3D reservoir modeling at Ram/Powell Field: A turbidite deposit in the eastern Gulf of Mexico: 1996 Society of Petroleum Engineers Annual Technical Coference and Exhibition.

Pfeiffer, D. S., B. T. Mitchell, and Y. Y. Gilbert, 2000, Mensa, Mississippi Canyon Block 731 Field, Gulf of Mexico - An integrated field study: GCSSEPM Foundation 20th Annual Research Conference: Deep Water Reservoirs of the World.

Van Kirk, C. W., 1976, Jormar - Reservoir performance and numerical simulation of a classic Denver-Julesburg Basin oil field: Rocky Mountain Regional Meeting of the Society of Petroleum Engineers.

Zambrano, G., A. Granado, and A. Rincon, 1968, A compositional simulation evaluation of the Santa Rosa, Colorado EF Reservoir, Eastern Venezuela: 63rd Annual Technical Conference and Exhibtion Society of Petroleum Engineers.

Chapter 3

Optimization of Recovery from the Popeye Reservoir

Overview

The Popeye reservoir is a two-layer reservoir with crossflow. A reservoir model has been created using seismic, well, fluid, and core data. The Popeye reservoir model is modified in order to match historical pressure and production data. Future recovery predictions from Popeye show bypassed reserves in the laminated portion of the RN and RM reservoir compartments. This chapter discusses the procedure used to history match the Popeye reservoir model and the effect of applying the production strategies described in Chapter 4 on the predicted recovery from Popeye.

Introduction

History matching uses historical production data to calibrate a reservoir model and improve confidence in predictions made using the reservoir model (Mattax and Dalton, 1990). A history match is accomplished by specifying a fluid production (or injection) rate (oil, water, or gas) or bottom-hole pressures for each well in the field. This controls production from each well in the field through time. Reservoir and fluid properties are modified until a match with the unspecified fluid production (or injection) rates or bottom hole pressures is reached for each well in the field (Ertekin et al., 2001). In history match simulations performed on the Popeye reservoir model, historical gas production was specified and the model input parameters was modified to match historical oil production, water production and pressure data.

The Popeye reservoir model was developed based on well, seismic, fluid, and core data. Appendix A and C summarize the seismic, geologic, and PVT data that constrains most of the reservoir model inputs. In addition, pressure transient analysis (PTA) protocols were used to evaluate the horizontal permeability of the producing reservoir (G-sand) at Popeye.

By monitoring the pressure response in a well during changes in the production rate, it is possible to determine the reservoir permeability (Horne, 1995). These techniques have been extended to determine the permeability of individual layers within layered reservoirs that have hydrocarbon production commingling in the wellbore (Ehlig-Economides and Joseph, 1987; Kucuk et al., 1986) and to reservoirs with crossflow that have a series of layers in communication away from the wellbore (Ehlig-Economides and Joseph, 1987).

At Popeye, the major uncertainty in reservoir properties is the vertical communication between layers; appropriate pressure transient analysis techniques would allow for the vertical permeability to be calculated. Unfortunately, the specific tests required for this type of analysis were not performed at Popeye.

Initial simulations at Popeye incorrectly predict the water breakthrough in the A2BP well (Fig. 3.1). Adjustment of the vertical permeabilities of each layer improves the match between simulator data and historical data. By going through the history matching procedure, further insight on Popeye has been gained and subsequently our understanding of fluid flow dynamics through the reservoirs of the Popeye field is enhanced.

The Popeye history matched reservoir model is used to test production optimization strategies predicted using the simple model in chapter four. Simulations using the

Popeye reservoir model show the recovery from two reservoirs would improve if only the laminated layer was perforated.

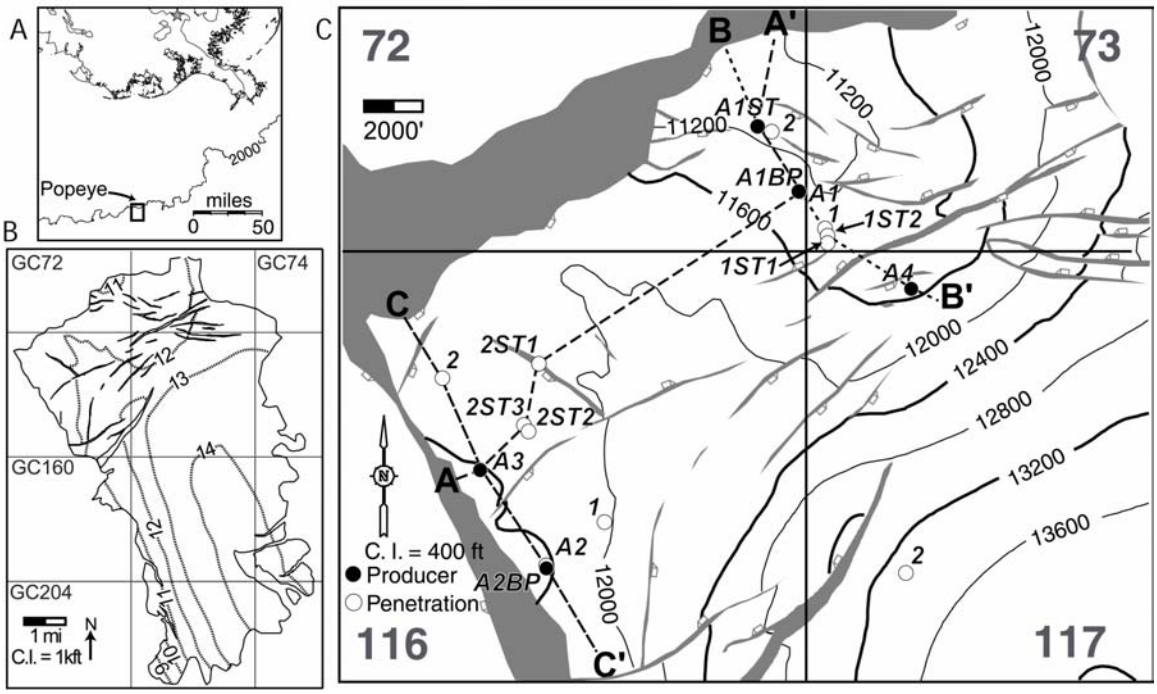

Adapted from Appendix C

Figure 3.1: A) The Popeye field is located 140 miles southwest of New Orleans in 2000 ft of water. B) Structure map of vertical subsea depth (TVDSS) to the top of the G-sand in the minibasin. This map was created by mapping the trough minima of the G-sand reflector and depth-converting it using known penetration depths at well locations (Appendix C). C) Expanded view of structure map, focused on the Popeye field.

Well / Reservoir	Date Production Began	Date Production Ended	Cumulative Production as of (06/25/2003) (BCF)	Current Production Rate (06/25/2003) (MMSCF)
A1BP / RA	01/01/1996	01/01/1999	47	0
A2BP / RM	01/01/1996	04/01/2002	125	0
A3 / RN	01/01/1998	-	68	20
A1ST / RA	01/01/1999	-	75	59
A4 / RB	04/01/2002	-	17	29

Table 3.1: Production history of the producing wells of the Popeye field. The locations of the wells are shown in figure 3.1. All wells are perforated in both the G_L and G_M when they initially begin production. The A3 well is only perforated in the G_L after June 2000 due to complications during a well workover.

Popeye Reservoir Model

The G-sand is the producing reservoir in the Popeye field; it produces gas and condensate from a laminated facies (G_L) that overlies a massive facies (G_M) (Fig. 3.2). Sixteen wells were drilled in the Popeye field; five are producers (Fig. 3.1, Table 3.1). For simulation, the G_L and G_M are represented by separate layers; each layer has distinct and constant rock properties (Table 3.2). Layer thicknesses are derived from Figure 3.3 and structural geometry from Figure 3.4. There are four hydrocarbon compartments located on structural highs (Fig. 3.4) of the field. These compartments are separated by sealing faults (Fig. 3.5) and an impermeable channel (Fig 3.4). A more detailed description of the Popeye reservoir model used in this study can be found in Appendix A and C.

Layer	Porosity (%)	k_h (mD)	k_v (mD)	Sw_{irr}	Sg_r	Net to Gross Ratio
G_L	25	500	0.1	0.143	0.021	0.6
G_M	30	1,200	500	0.119	0.022	1.0

Table 3.2: Constant Property Values Assigned to Simulation Layers in Reservoir Model

Using PTA to Constrain Horizontal Permeabilities

The horizontal and vertical permeabilities for the two layers of the Popeye reservoir model are the most difficult to constrain. The values of 500 mD for the horizontal permeability of G_L (k_{hL}) and 1,200 mD for the horizontal permeability of the G_M (k_{hM}) were initially assumed. Pressure transient analysis is used to evaluate the validity of these assumptions.

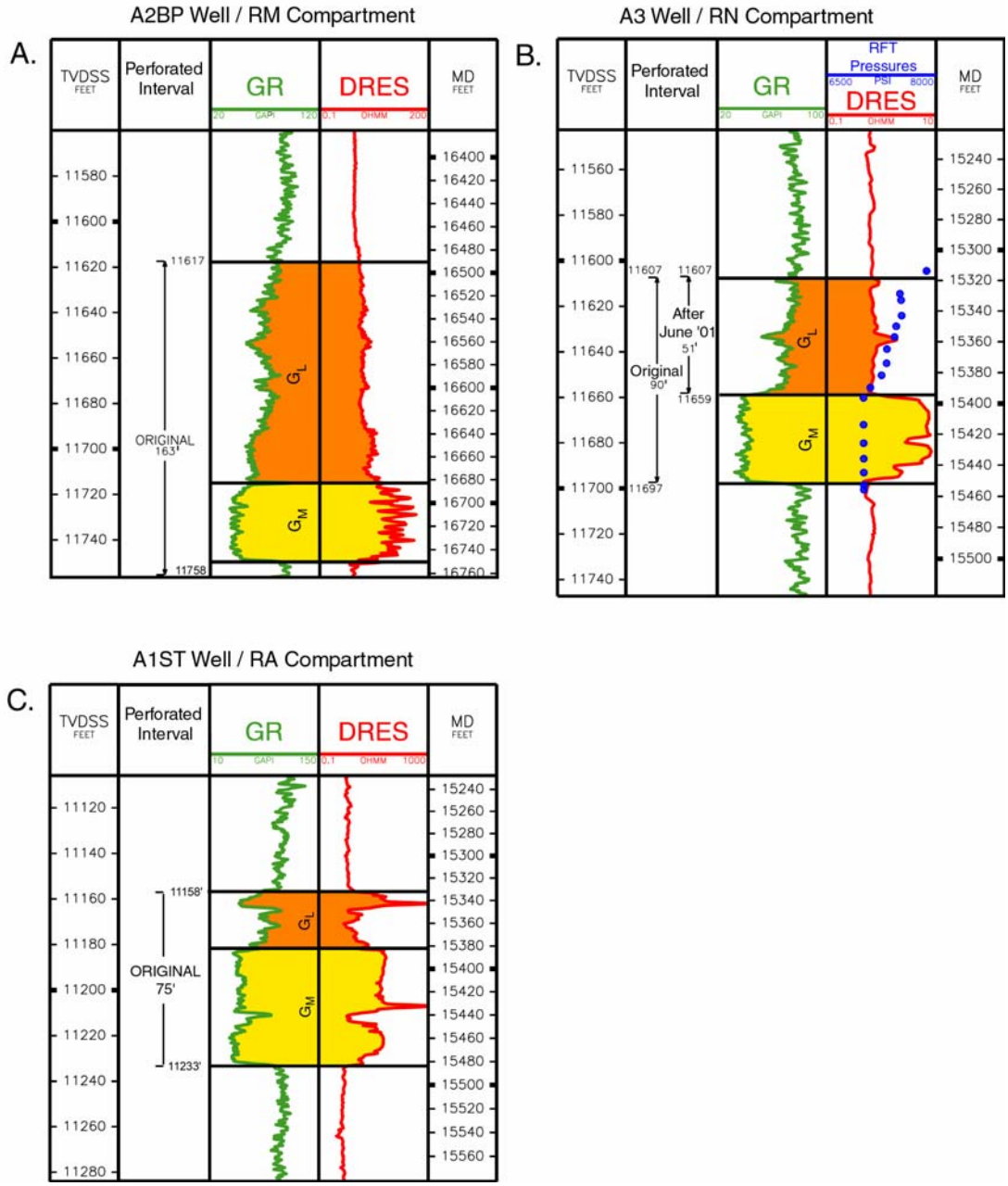

Figure 3.2: A) Gamma ray and resistivity log for the A2BP well which also shows the perforated intervals and the date the perforations began. B) Gamma ray and resistivity log for the A3 well which also shows the perforated intervals and the date the perforations began. The ramped gamma ray signature in the laminated portion of the A2BP well compared to the flatter consistently higher gamma ray signature in the laminated portion of the A3 well suggests the laminated portion of the RM compartment is of equal or higher quality then the RN compartment (Fig 3.4). C) Gamma ray and resistivity log for the A1ST well. Notice the large difference in laminated sand compared to massive sand.

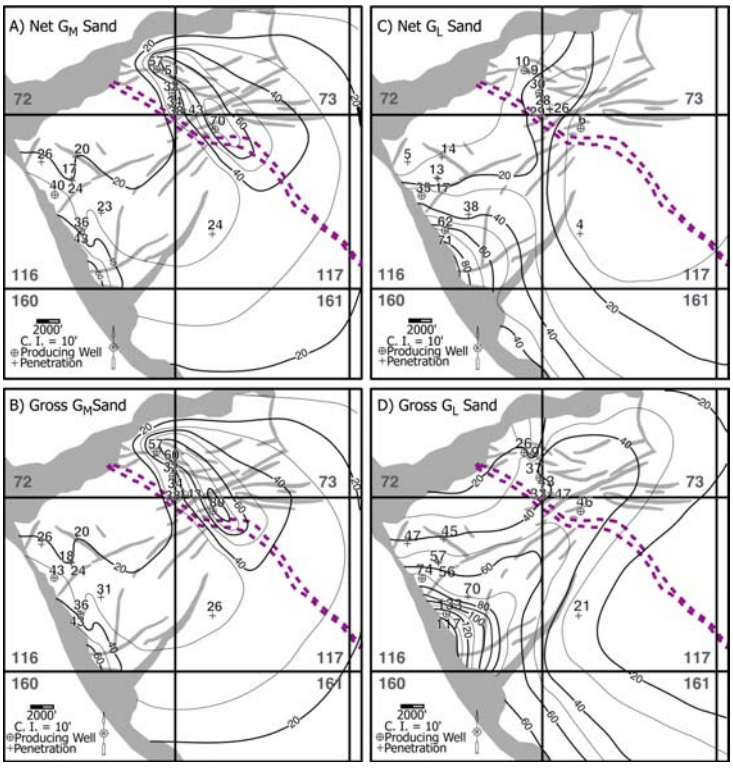

Adapted from Appendix C

Figure 3.3: Net and gross G-sand thicknesses based on well data, seismic reflection character and depositional model Appendix C. A and B) Net and gross G_M distributions are similar due to the high G_M net-to-gross ratio. C and D) Thickest net and gross G_L are located in the RM reservoir.

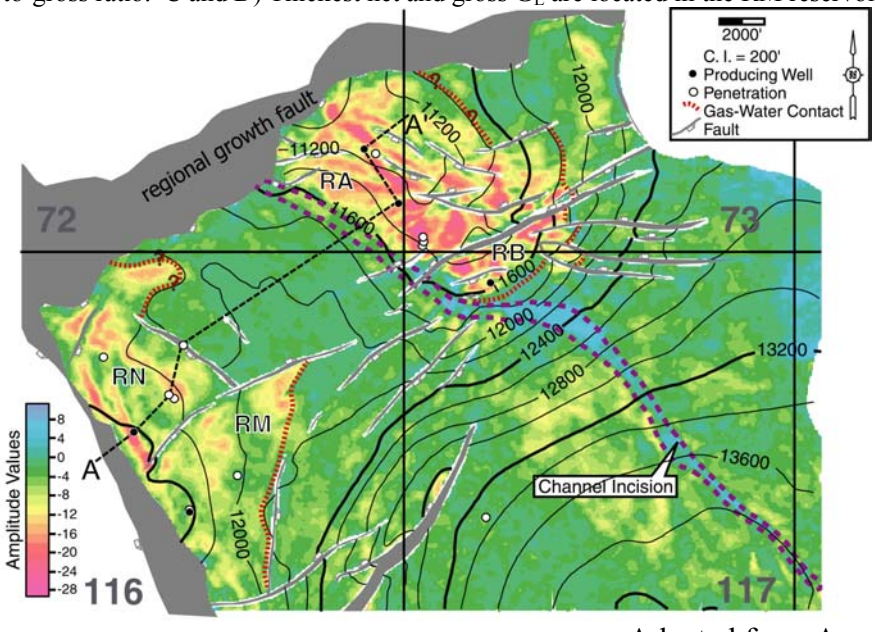

Adapted from Appendix C

Figure 3.4: The amplitude of the G-sand trough with contours of the depth (TVDSS) to the top of the G_L (Appendix C). The channel incision is interpreted to be impermeable.

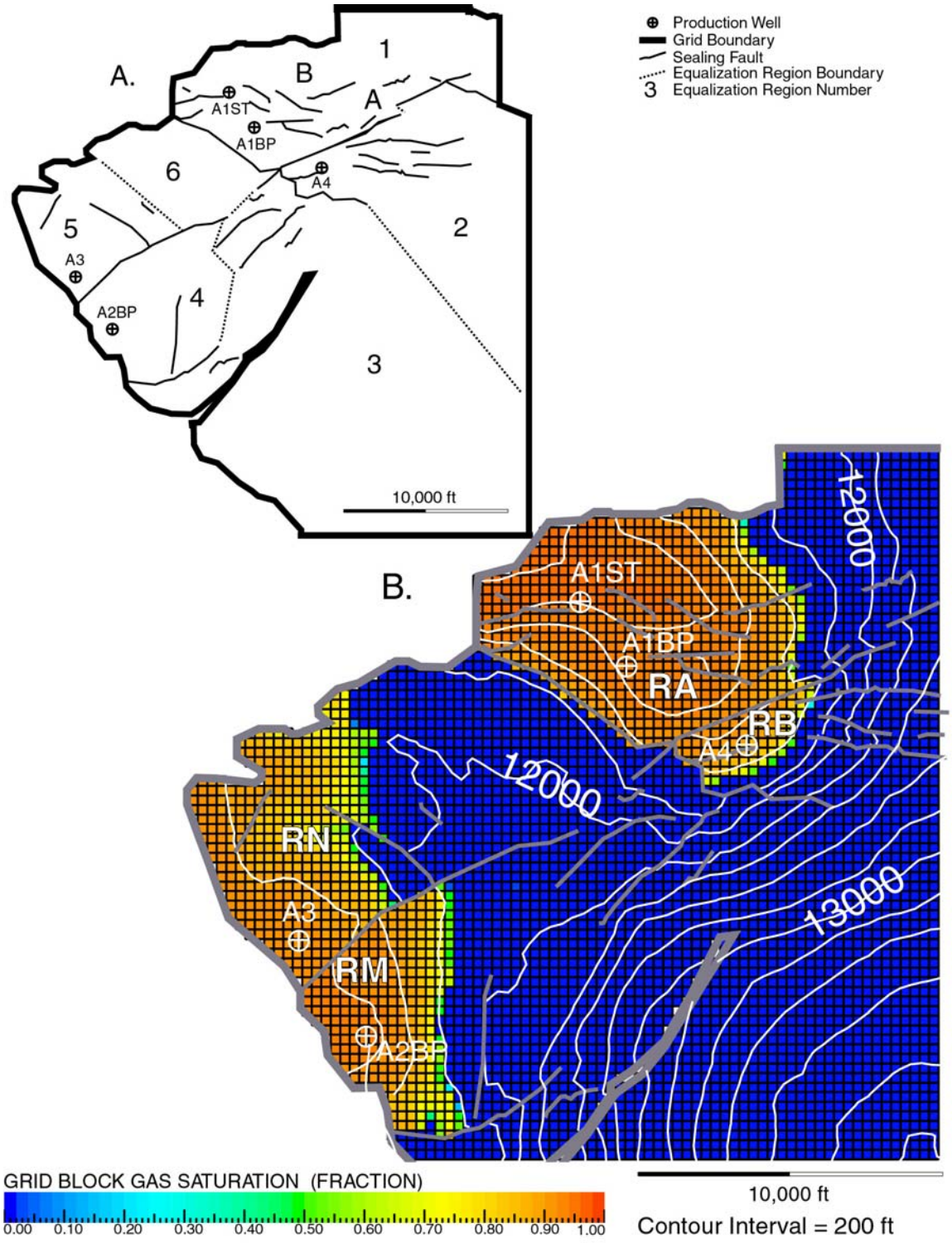

Figure 3.5: A) Equalization regions and boundary conditions for the Popeye reservoir simulator. The hydrocarbon bearing regions are 1, 2, 4, and 5; 3 and 6 are aquifer regions. B) Initial gas saturation in the G_M layer (01/01/1996). Initially there is 761 BCF gas in place.

Well	Gross Thickness		Total G-sand Thickness	Perforation Dates			
	L	M		L		M	
				Start	Finish	Start	Finish
A2BP	92	40	132	01/01/96	04/01/02	01/01/96	04/01/02
A3	52	38	90	01/01/98	-	01/01/98	06/01/98

Table 3.3: Gross thickness and dates perforated for G_L and G_M in the A2BP and A3 wells.

Accordingly, pressure transient analysis (PTA) was performed in the A2BP and the A3 wells (Fig. 3.2) to assess the average horizontal permeability of the G_L ($k_h avg_L$) and the G_M ($k_h avg_M$) (Fig. 3.6). The thicknesses of the G_L and the G_M and the layers perforated vary between the RN and RM reservoir compartments.

The A2BP well (RM) has 92 ft of G_L and 40 ft of G_M; the A3 (RN) well has 52 ft of G_L and 38 ft of G_M (Fig. 3.2, Table 3.3). Well A2BP is perforated in both the G_L and G_M throughout the life of the well (01-01-96 to 04-01-02) (Fig. 3.2A, Table 3.3); the A3 well was originally (03-01-98) perforated in both layers but workover complications in June 2001 resulted in only the G_L being perforated (Fig. 3.2B, Table 3.3).

Horizontal permeabilities were calculated for the G_L and the entire G-sand in the A2BP and A3 (Fig 3.1) wells by performing PTA on pressure build-ups. The pressure build-ups were extracted from continuous bottom-hole pressure gauge data. Figure 3.7 and 3.8 show the semilog plots used to determine the slope of the straight line formed during the initial infinite-acting portion of the data. This slope, in combination with the average net thickness of the reservoir (Table 3.4), allows for the average horizontal permeability of the perforated interval to be calculated using the equation

$$k_h avg_x = \frac{1.632 \times 10^6 q_{sc} T}{m h_x}. \qquad 3.1$$

where $k_h avg_x$ is the average horizontal permeability of the perforated interval, x is G (entire G-sand) or L (laminated layer) depending on the perforated interval, 1.632×10^6 is a unit conversion factor, q_{sc} is the average flow rate until the time the build-up test begins, T is the reservoir temperature in Rankin, m is the slope of the semilog straight line, and h_x is the average net thickness of the tested reservoir.

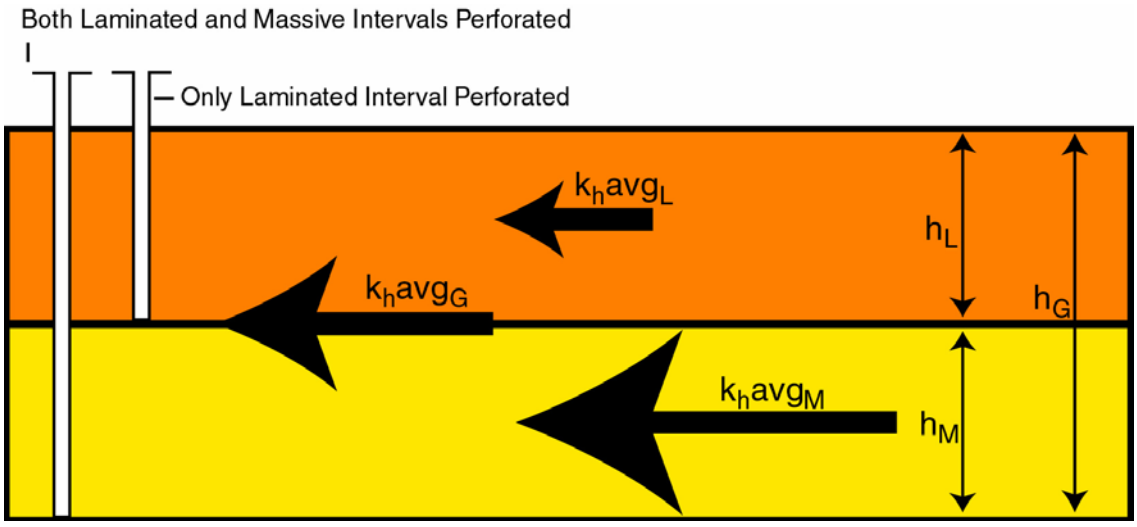

Figure 3.6: Graphical description of the average horizontal permeabilities ($k_h avg_G$, $k_h avg_L$, and $k_h avg_M$) of the G-sand, net thicknesses of the G-sand (h_G, h_L, and h_M) and perforation schemes.

A.

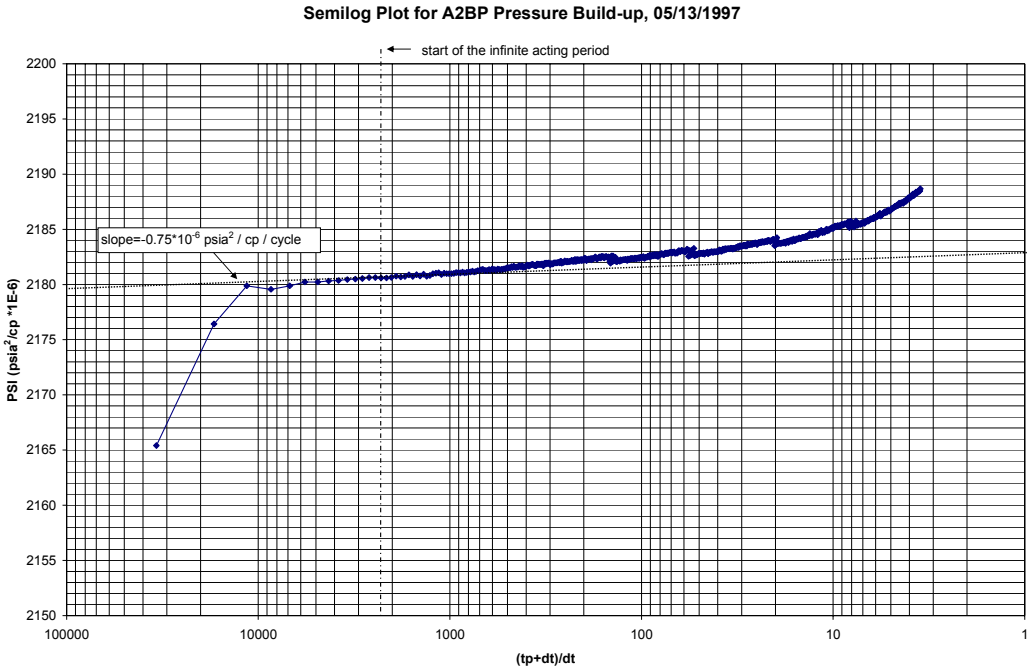

B.

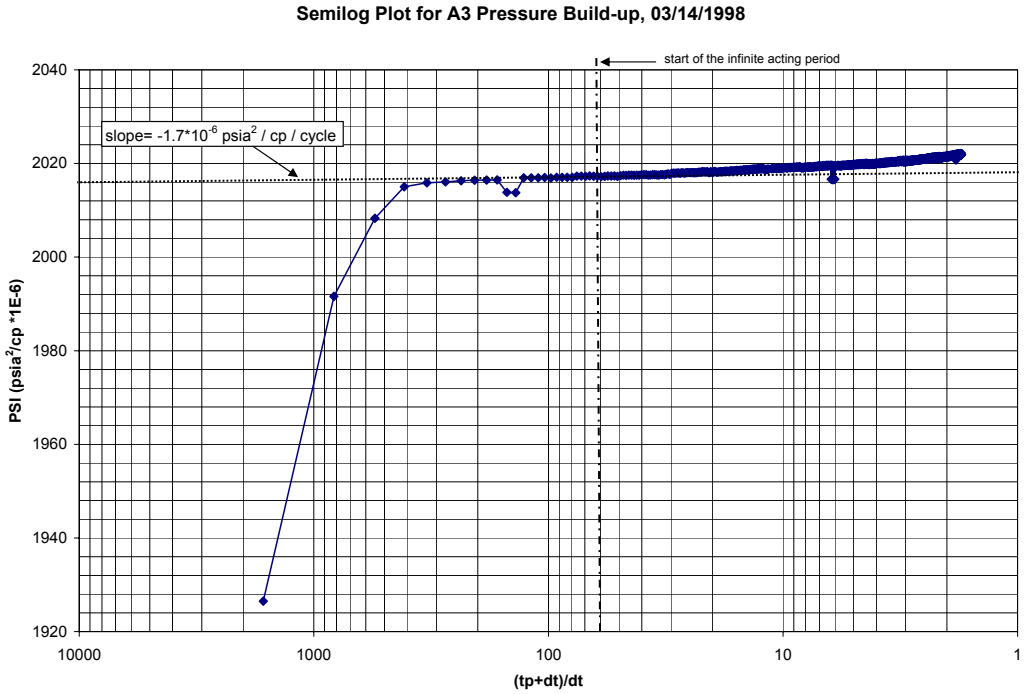

Figure 3.7: Semilog plots for A2BP and A3 wells at 05/13/97 and 03/14/98 respectively. Each well is perforated in both the laminated and massive layers while this data is collected. The increase in pressure at late time suggests there is pressure support due to crossflow between the layers.

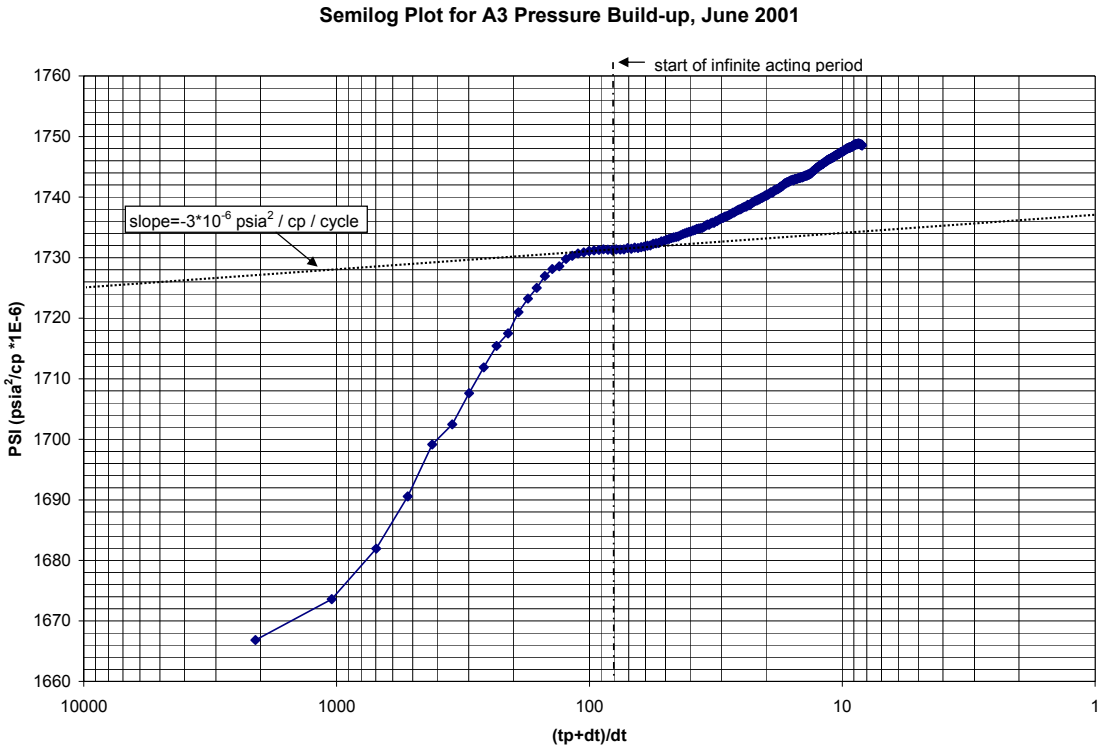

Figure 3.8: Semilog plot for the A3 pressure build-up in June 2001. Only the laminated portion of the G-sand is perforated during data collection. The increase in pressure at late time suggests there is pressure support due to crossflow between the layers.

The calculation of $k_h avg_M$ from $k_h avg_L$ and $k_h avg_G$ assumes that crossflow does not affect the slope (m) of the initial semi-log straight line used to calculate $k_h avg_G$. This is valid as long as the data used to determine the slope of the infinite acting flow period is collected while one-dimensional radial flow is present in the perforated intervals of the G-sand. Each of these build-up datasets show an initial infinite acting semi-log straight line portion (Fig. 3.7 and 3.8) followed by an increase in pressure support that is interpreted to be a result of crossflow. This suggests that initially a one-dimensional radial flow period exists and the condition is met. Therefore, $k_h avg_G$ should simply be and average of $k_h avg_L$ and $k_h avg_M$ (Eq. 3.1).

Two pressure build-up datasets, one from the A2BP well and one from the A3 well (Fig. 3.7), were used to determine average horizontal permeabilities for the entire G-sand

($k_h avg_G$) (Fig. 3.6). The $k_h avg_G$ was calculated to be 1,767 mD in the A3 well and 773 mD for the A2BP well (Table 3.4). The difference in $k_h avg_G$ between the A3 and A2BP well is expected because the contribution from each layer (G_L and G_M) to the average G-sand permeability ($k_h avg_G$) differs due to the large difference between laminated and massive sand thickness between the wells (Fig. 3.2).

The average horizontal permeability of the G_L ($k_h avg_L$) is calculated using a pressure build-up dataset during the period when only the laminated portion of the A3 well is perforated (Table 3.4, Fig. 3.6). Again, the pressure build-up data is analyzed by determining the slope of the semilog straight line formed during the infinite acting period (Fig. 3.8) and calculating the average horizontal permeability using the average net thickness of the laminated layer for the RN reservoir (Eq. 3.1, Table 3.4). This procedure assumes that the initial infinite acting period on the semilog plot is only responding to the G_L and that there are no effects from the G_M; $k_h avg_G$ equals $k_h avg_L$. The average horizontal permeability of the G_L ($k_h avg_L$) was calculated to be 604 mD (Table 3.3).

Well / Reservoir (Fig. 3.4)	**Date of Build-up**	**Perforated? (Y/N)**		**Permeability Calculated using PTA (mD); $k_h avg_G$**	**Average Reservoir Net Thickness (ft)**		**Calculated Massive Average Horizontal Permeability (mD); $K_h avg_M$**
		L	**M**		**L**	**M**	
A3 / RN	3-14-98	Y	Y	1,269	15	20	1,767
A3 / RN	June 01	Y	N	604 = **$k_h avg_L$**	15	20	N/A
A2BP /RM	5-13-97	Y	Y	773	62	30	1,122

Table 3.4: Results of average permeability calculation and pressure transient analysis. L denotes values for the laminated layer and M denotes values for the massive layer. The June '01, A3 calculated K_M is not applicable because this is when the well is only perforated in the laminated layer.

Reservoir Layer	k_h Used For Simulation (mD)
G_L	500
G_M	1,200

Table 3.5: Horizontal permeability (k_h) used for G_L and G_M in the Popeye reservoir simulator

The equation for average horizontal permeability is

$$k_h avg = \sum_{n=1}^{l} \frac{k_{hn} b_n}{b}, \qquad 3.2$$

where $k_h avg$ is the average horizontal permeability, k_{hn} is the horizontal permeability of the n^{th} layer, b_n is the thickness of the n^{th} layer, and b is the total net thickness. Assuming the $k_h avg_L$ value (604 mD) is homogenous across the field and using the $k_h avg_G$ values from when both layers of the G-sand are perforated in each well allows for the calculation of $k_h avg_M$ (Eq. 3.2). The net thicknesses in Table 3.4 were used to calculate a $k_h avg_M$ of 1,767 mD in the A3 well and 1,122 mD in the A2BP well.

PTA calculations determine $k_h avg_L$ equals 604 mD and using this value and PTA determined $k_h avg_G$ values, $k_h avg_M$ is determined to be between 1122 and 1767 mD. However, during the pressure build-up tests, pressure transients do not reach the entire reservoir. Therefore, a reduced average reservoir thickness should be used to calculate $k_h avg_L$ and $k_h avg_G$ (Eq. 3.1) because the thickness of the reservoir decreases away from wells A3 and A2BP (Fig. 3.3). Taking the reduced average reservoir thickness into account makes the values of horizontal permeability used in the Popeye reservoir model (k_{hL} = 500 mD in G_L and k_{hM} = 1200 mD in G_M) reasonable.

Ram/Powell (Clemenceau et al., 2000) and Tahoe (White et al., 1992) are Gulf of Mexico fields with reservoirs in levee-overbank deposits similar to G_L (Appendix C). Reservoir simulation and PTA were used to establish 35 mD as the average horizontal permeability of the L reservoir at Ram/Powell and the producing sand of the Tahoe field. The average horizontal permeability of the G_L at Popeye ($k_h avg_L$ = 604 mD) is significantly greater than the L-sand at Ram/Powell and the reservoir sand at Tahoe. However, $k_h avg_L$ of the G_L does agree with the estimated permeability of the laminated portion of the J-sand at Ram/Powell (an amalgamated channel and sheet sand complex with 300 mD to 600 mD permeability) (Lerch et al., 1996) and other fields in the Gulf of Mexico (300 mD average) (Slatt et al., 1998). The RN compartment (Fig. 3.4) well logs (A3 included) show the lowest quality G_L (Appendix C), which leads to the interpretation that the average permeability of the laminated layer in the RM reservoir is equal or higher (Fig. 3.2).

The $k_h avg_M$ of the G_M determined using PTA (1,767 mD and 1,127 mD) and used in the reservoir model (1,200 mD) agree with permeabilities of similar facies from various fields across the Gulf of Mexico. Fields such as Genesis (Rafalowski et al., 1994), Ram/Powell (Lerch et al., 1996), Mensa (Pfeiffer et al., 2000) and Bullwinkle (Holman and Robertson, 1994) have hydrocarbon accumulations in massive amalgamated sheet sand deposits similar to the massive portion of the G-sand. The N3 sand at Genesis is composed of amalgamated channel sands with a horizontal permeability of 3000 mD (Rafalowski et al., 1994). The Ram/Powell field produces from the J-sand; a portion of which is characterized as a massive amalgamated channel and sheet sand with horizontal permeabilities ranging from 900 mD to 1,200 mD (Lerch et al., 1996). Horizontal

permeabilities of the I sand at the Mensa field, an amalgamated sheet sand deposit, range from 500 mD to 2,000 mD (Pfeiffer et al., 2000). Holman and Robertson (1994) describe the J sands of the Bullwinkle field as amalgamated channel and sheet sand deposits that have horizontal permeabilities between 700 mD and 2,700 mD.

History Match of the Popeye Field

A three-dimensional, compositional reservoir simulator is used to match production and pressure data. Obtaining a history match required adjustment of the gas-water contacts (GWCs) of each reservoir and vertical communication between the laminated and massive layers.

Originally, simulations were run using the GWCs interpreted from seismic data, horizontal permeabilities that are in close agreement with PTA results, and zero vertical permeability between the two layers. This resulted in early and too strong of a water breakthrough in the A2BP well (Fig. 3.9). The history match was improved by assigning an average vertical permeability of 0.1 mD to the laminated layer and 500 mD to the massive layer (Table 3.4, Fig. 3.9). If there is no vertical communication between the layers and the PTA constrained horizontal permeability values are used, then, the GWC in the RM reservoir would have to extend beyond what is practical from the seismic data interpretation (Fig. 3.4). These vertical permeability values are considered constant across the field because they improved the pressure match in all of the other producing wells.

The final history match was achieved by modifying the GWCs in each of the reservoirs (Fig. 3.10). This further improved the match between simulated bottom-hole

pressures and historical data. The adjustments were small (<10 vertical feet) and remain consistent with the GWCs predicted by the 3D seismic data (Fig. 3.4).

In the final history match, the horizontal to vertical permeability ratio (k_v/k_h) for the laminated sand was 2×10^{-4} and for the massive sand was 0.42. The k_v/k_h assigned to the J-sand at Ram/Powell was 0.001 for the laminated facies and 0.95 for the massive facies (Lerch et al., 1996) and 0.01 for the I sand (massive amalgamated sheet) of the Mensa filed (Pfeiffer et al., 2000). The Popeye values are significantly lower than the J-sand values at Ram/Powell but are still considered reasonable because of the confidence in the PTA determine horizontal permeability values and GWCs interpreted from seismic data that constrain the reservoir model used for history matching.

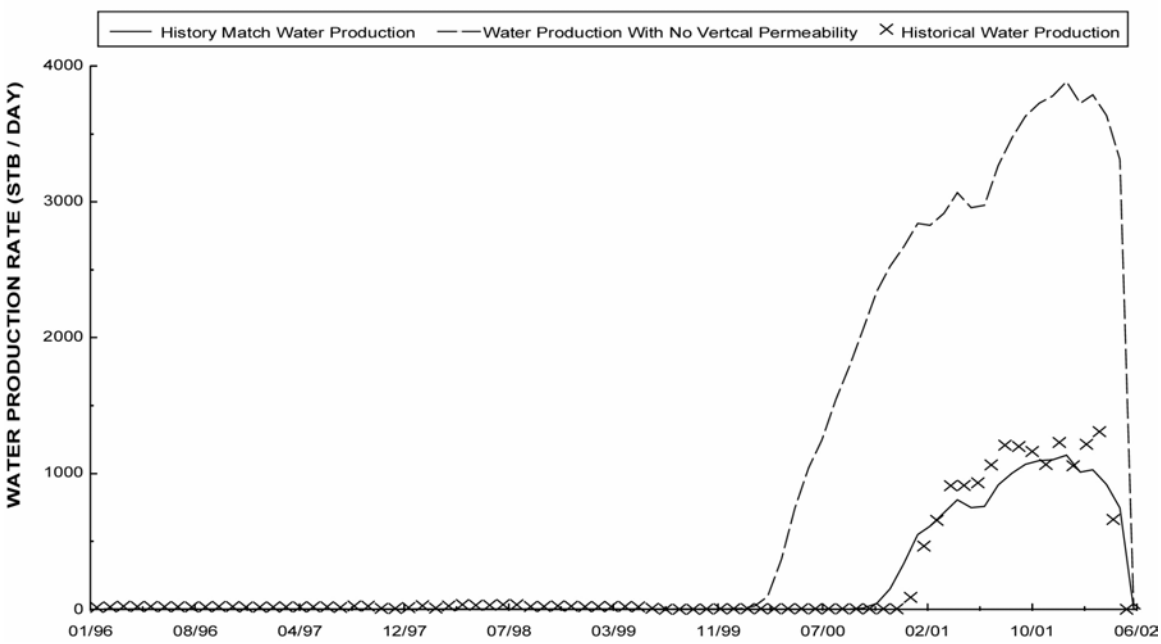

Figure 3.9: Difference in history match for simulations of the Popeye field that have no vertical communication between simulation layers and a simulation using a vertical permeability of 0.1 mD for the laminated layer and 500 mD for the massive layer.

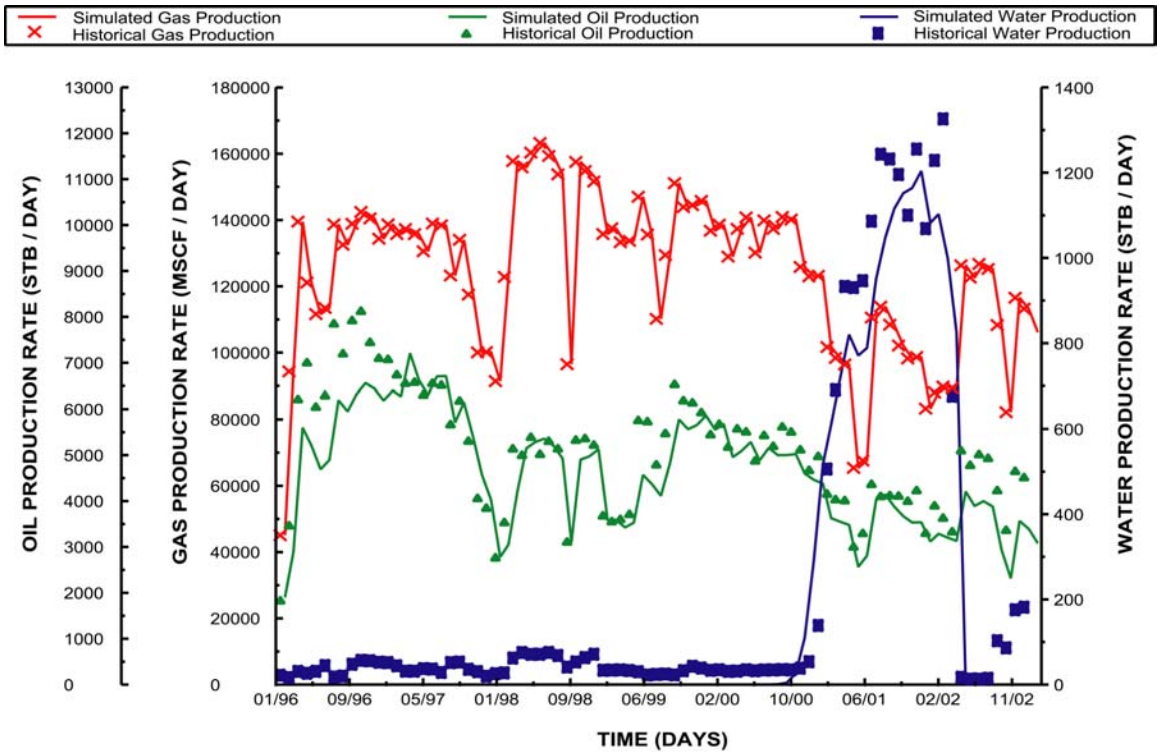

Figure 3.10: History match for the Popeye field from January 1996 to December 2002.

Recovery Predictions for Popeye Reservoir Model

Now that a history match has been performed predictions can be made that estimate the recovery from each reservoir compartment and locate areas of bypassed reserves. As shown in Chapter 3 the predicted recovery form each of the Popeye reservoir compartments depends on the k_{hL}/k_{hM}, k_{vL}/k_{vM}, and h_L/h_M of each compartment. In the Popeye reservoir model, all three of the reservoir compartments (RA, RN, and RM) have a k_{hL}/k_{hM} of 0.4167 and k_{vL}/k_{vM} of 0.0002. However, h_L/h_M varies for each reservoir compartment. In the RA compartment, the RN compartment, and the RM compartment h_L/h_M is 0.2, 1.0 and 1.85, respectively. Simulations performed using the Popeye reservoir model and historical production data predict gas recoveries of 72% in the RA reservoir, 52% in the RM reservoir and 73% in the RM reservoir. The percent recovery for the entire field is 59%.

The low recovery in the RM compartment can be attributed to the large amount of bypassed reserves in the RM compartment due to the high h_L/h_M (≈ 1.85) (Chapter 3 and Fig 3.11). The RN compartment does not show any bypassed reserves (Fig. 3.11). The RA compartment recoveries are higher than in the RN and RM compartments. The predicted saturation distributions of the RA reservoir at the end of the field life (Fig. 3.11C) do not show any reserves in the laminated layer that could be targeted by only producing from the laminated layer.

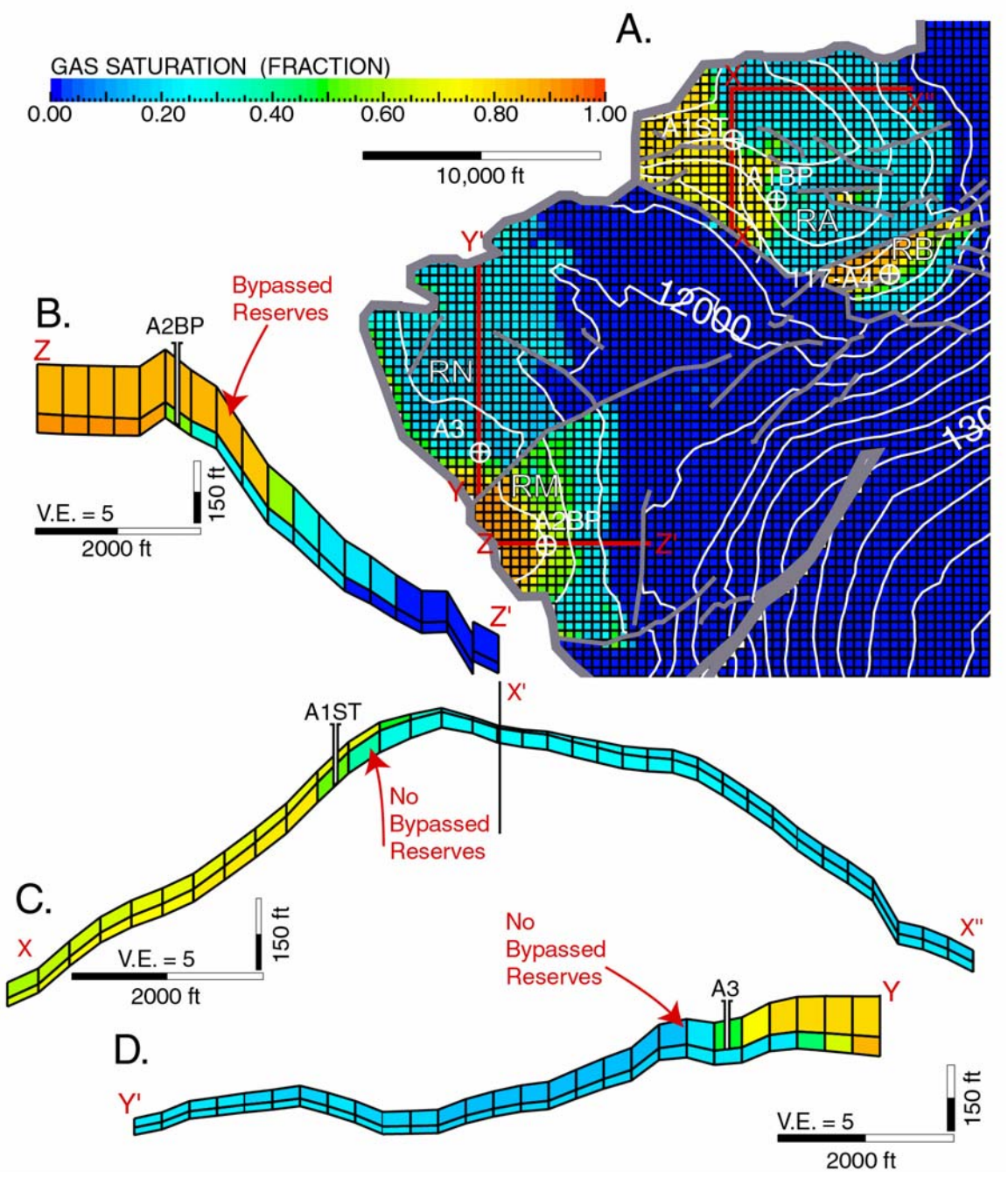

Figure 3.11: A) Final Saturation distribution of the G_M in the Popeye field after 28 years of production. For this simulation both G_M and G_L of the reservoir are perforated in the A2BP and A1ST wells. The A3 well is only perforated in the G_L. This is consistent with the production history of the field. For all the cross-sections the G_L is above the G_M. B) Cross-section through the RM reservoir showing an area of bypassed reserves in the G_L when water reaches the well bore in the G_M. C) Cross-section of the RA reservoir. Notice the reservoir is completely swept in both the G_L and G_M when both layers of the reservoir are perforated. D) Cross-section of the RN reservoir showing that no bypassed reserves are left behind due to the A3 well only being perforated in the G_L. Production history is in Table 3.1.

Applying Optimization Results to Popeye

New simulations for the Popeye field were run in order to compare the perforation strategy predictions of the optimization protocol with results from Popeye. The Popeye reservoir model was not changed but the well constraints are modified from the history-match case (Table 3.6) to match those of the optimization protocol simulations. The specified gas rates of the producing wells are changed to maximum rates rather then historical rates. The maximum rate of each well is achieved by specifying an unreasonably high flow rate and using a drawdown constraint of 300 psi to limit the amount of production from the well. Additionally, the wells are connected to a manifold within a surface pipeline network. A minimum pressure at the manifold limits the bottom-hole pressure for each of the producing wells and controls the abandonment pressure of the well.

The new Popeye simulations include one with both layer perforated in the RN, RM and RA reservoir compartments. The results from these simulations are then compared to the results from simulations that only perforate the laminated in the RN, RM and RA reservoir compartments. By comparing the recovery difference (*RD*) (Eq. 2.1) from these simulations with the *RD* predicted by the optimization protocol, insight can be gained into the accuracy of the predicted recovery increases from the optimization protocol.

Well Constraint	Value
Gas Flow Rate	Maximum rate allowed by drawdown constraint
Pressure Drawdown Constraint	300 psi
Manifold Pressure Constraint	1,515 psi

Table 3.6: Well constraints used for Popeye simulations that compare recovery of only perforating the laminated layer in each reservoir compartment and the recovery of perforating both layers of each reservoir compartment.

Simulations performed with both layer of the reservoir perforated show bypassed reserves in the RN and RM reservoir compartments and no bypassed reserves in the RA compartment (Fig. 3.12). There are fewer reserves bypassed in the RN compartment (Fig. 3.12C) than in the RM compartment (Fig. 3.12B). The history-match Popeye simulation predictions suggest that only perforating the laminated layer of the RN compartment would reduce the amount of bypassed reserves (Fig. 3.11). Simulations performed with only the laminated layer perforated in the RN, RM and RA compartments show the bypassed reserves are produced in the RN and RM compartments and that reserves are bypassed in the RA compartment (Fig. 3.13).

The difference in recovery due to the two different perforation strategies is quantified by calculating the *RD* of each reservoir compartment (Table 3.7). *RD* is -9.81, -12.73 and 59.24 for the RM, RN and RA reservoir compartments, respectively.

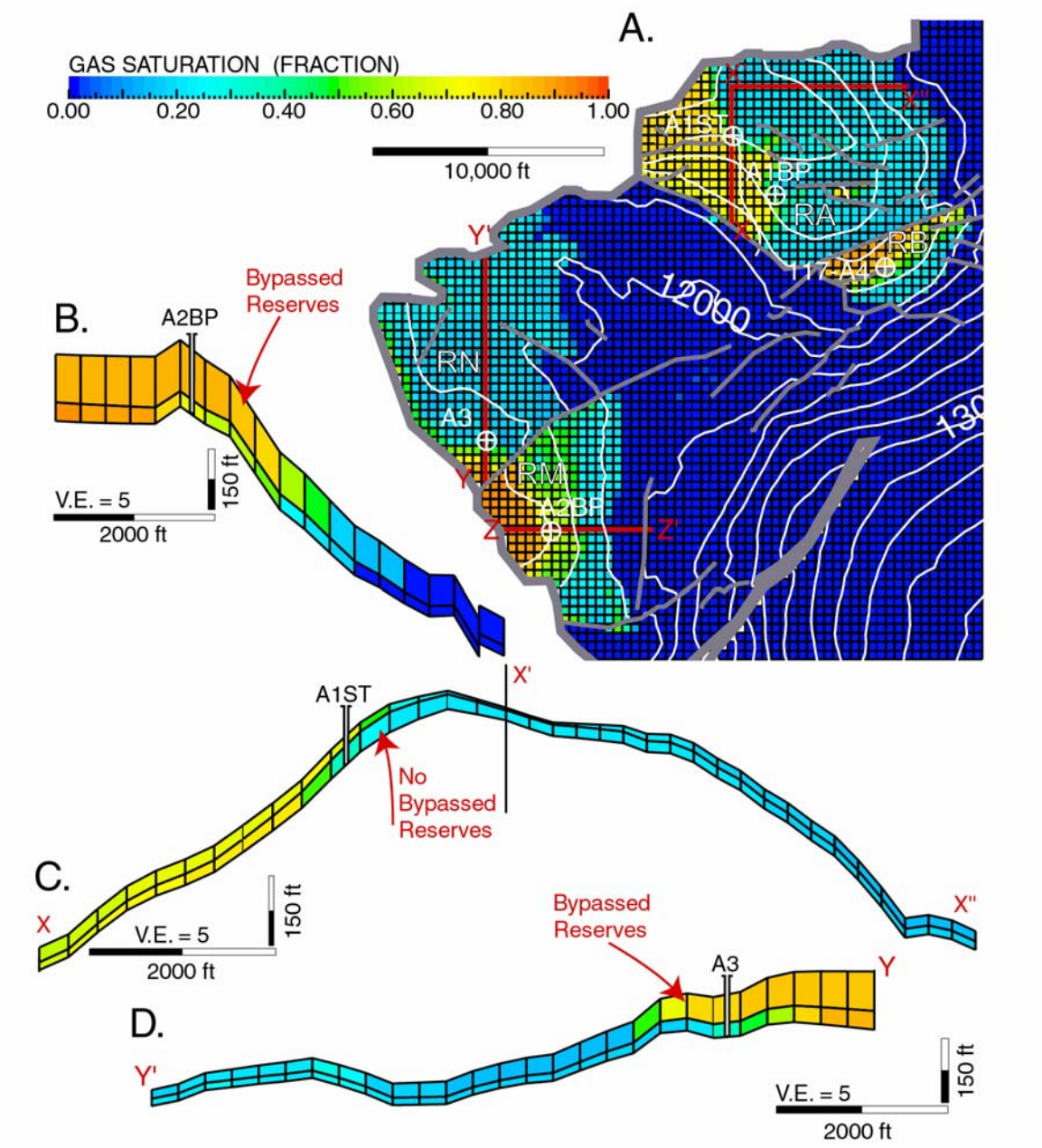

Figure 3.12: A) Final Saturation distribution of the G_M in the Popeye field after 28 years of production. For this simulation both layers of the reservoir are perforated in the producing wells. For all the cross-sections the G_L is above the G_M. B) Cross-section through the RM reservoir showing an area of bypassed reserves in the G_L when water reaches the well bore in the G_M. C) Cross-section of the RA reservoir. Notice the reservoir is completely swept in both the G_L and G_M when both layers of the reservoir are perforated. D) Cross-section of the RN reservoir showing an area of bypassed reserves in the G_L.

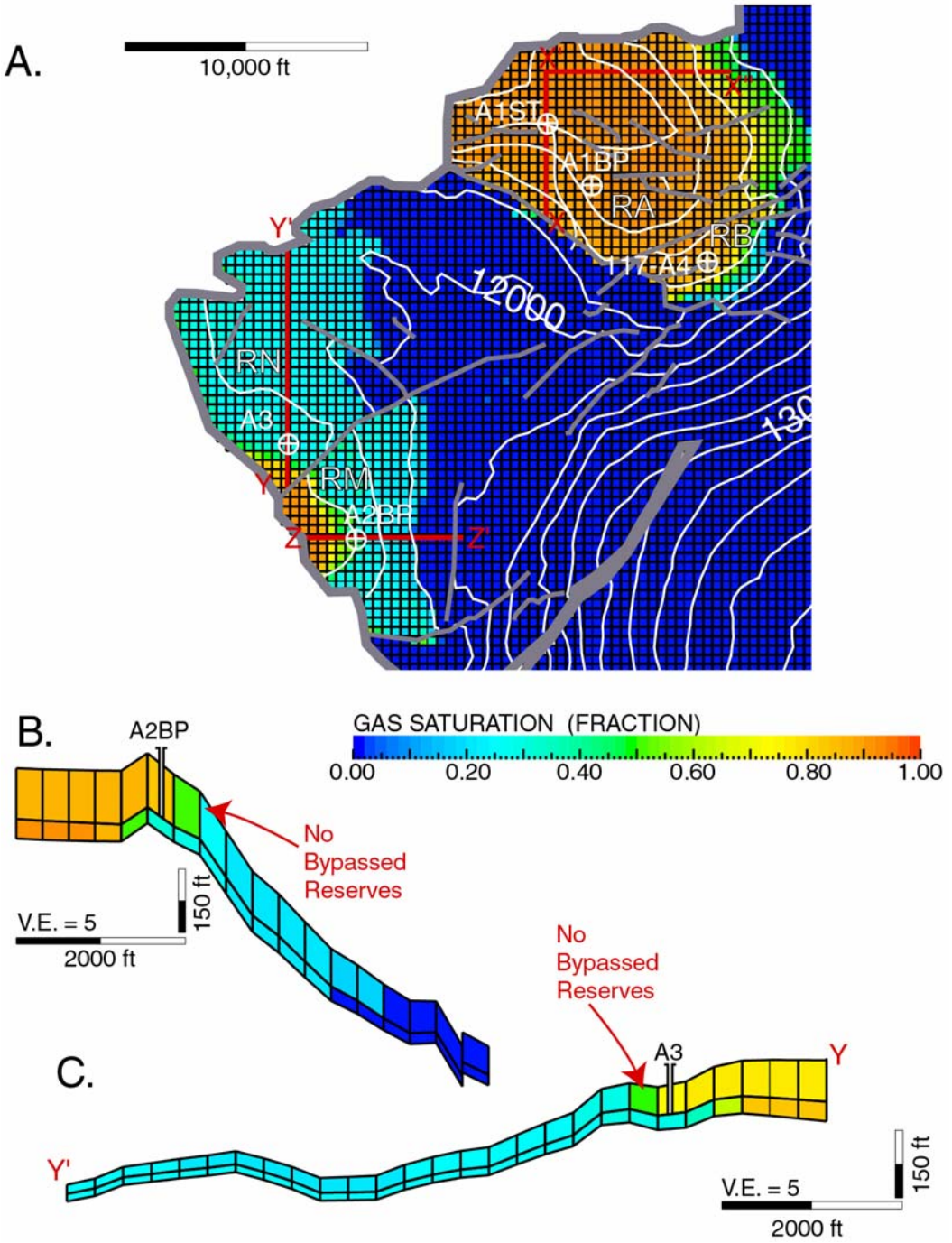

Figure 3.13: A) Final Saturation distribution of the G_M in the Popeye field after 18 years of production. For this simulation only the G_L is perforated in the producing wells. For the cross-sections the G_L is above the G_M. B) Cross-section through the RM reservoir showing both the G_L and G_M are efficiently swept. C) Cross-section of the RN reservoir showing both the G_L and G_M are efficiently swept.

Evaluation of the Optimization Protocol

Each of the reservoir compartments of the Popeye field has a k_{hL}/k_{hM} of 0.42 and a k_{vL}/k_{vM} of 0.0002; the value of h_L/h_M is 1.0, 1.85 and 0.2 in the RN, RM and RA reservoirs, respectively. The optimization protocol predicts that perforating only the laminated layer would increase production form the RN and RM reservoirs but would decrease production from the RA reservoir (Fig. 3.14A). Perforating the laminated layer of the RN and RM reservoir should increase recovery by 7.8 % and 8.0 %, respectively (Table 3.7). Perforating the laminated layer of the RA reservoir shows a decrease in recovery of 32 % (Table 3.7).

Reservoir Compartment / Producing Well	Actual *RD* From Popeye Simulations	*RD* Predicted From Optimization Protocol
RM / A3	-9.18	-7.8
RN / A2BP	-12.73	-8.0
RA / A1ST	59.24	32.0

Table 3.7: Table comparing values of *RD* between those calculated from Popeye simulations and those predicted by the optimization protocol (Chapter 3).

The increase in recovery due to perforating only the laminated layer in the RN and RM reservoirs predicted by the optimization protocol compares well to the values calculated from the Popeye simulations (Table 3.7). The differences between these results can be attributed to the simple model used to create the optimization model not being an exact replica of each reservoir within the Popeye model. The good comparison between actual results and those predicted by the optimization protocol suggest that the optimization protocol is a good tool for predicting recovery increases due to only perforating the laminated layer of a two-layer reservoir with crossflow.

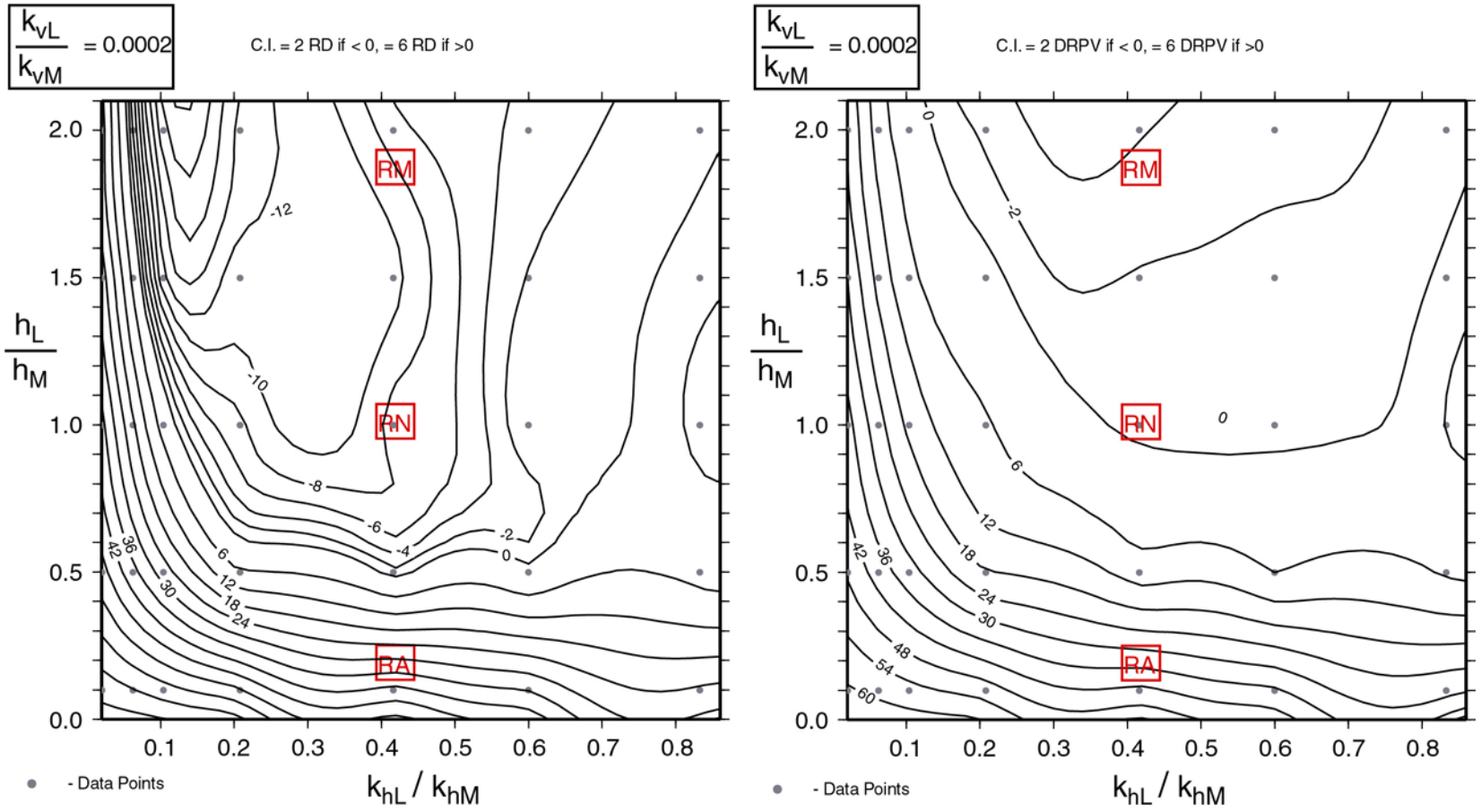

Figure 3.14: (A) *RD* contour plot for k_{vL}/k_{vM} equal to 0.0002 and various values of h_L/h_M and k_{hL}/k_{hM}. This plot was interpolated from the optimization protocol plots for k_{vL}/k_{vM} values equal to 0.0005 and 0.0004. (B) *DRPV* (Eq. 2.1) contour plot for the same simulation as (A) but the recoveries are discounted based on a 7% discount rate used for the *RPV* calculations (Eq. 2.2). Contour plot B shows the results of performing the economic calculations (*RPV* and *DRPV*) on the simulation results used to produce contour plot (A).

There is not a good comparison between the recovery differences predicted by the optimization protocol and the results calculated from the RA reservoir (Table 3.7). This difference in results is due to a difference in the amount of time wells are allowed to produce for in both the optimization protocol simulations and the Popeye simulations. Wells are allowed to produce for two different time spans in optimization protocol simulations and the Popeye simulations. Therefore, the total recovery at the end of simulation is different and the *RD* calculations are going to have different results (Table 3.7). With the reservoir conditions of the RA reservoir (Fig. 3.14A) the time it takes to produce the reserves with only the laminated layer perorated compared to both layers perforated makes it obvious that perforating both layers is the optimal production strategy. In these cases the best perforation strategy is predicted by the optimization protocol, even though the magnitude of the recovery difference is not correct.

Economic Impact of Only Perforating the Laminated Layer at Popeye

The economic impact of only producing from the laminated layers of the RN and RM reservoirs has to be considered before a perforation strategy decision can be made. There is a significant impact on the expected recoveries of the RN and RM reservoirs when the time-value of money is considered (Fig. 3.14B). A discounted recovery difference (*DRPV*) was calculated for the RN and RM reservoirs using a 7% discount rate (*r*) for *RPV* calculations (Table 3.8). According to the results of the economic calculation, perforating the laminated layer in both the RN and RM reservoirs is economically justified.

The *DRPV* results calculated for the RN and RM compartments do not match well with the *DRPV* results predicted by performing economic calculations on the results predicted by the optimization protocol (Fig. 4.14B, Table 3.8). The reason for the difference in results is due to the manifold pressure constraint on the wells in the Popeye field (Table 3.6). All of the wells in the Popeye field are joined to a subsea manifold where fluids from the wells commingle and are transported onshore through a single flow line. The pressure at this manifold controls the maximum rate of all the wells in the Popeye field. As a result, the wells within the Popeye field are not allowed to produce at as high of rates as if they were not connected to the manifold.

Production when both layers of the reservoir are perforated is effected the most by the reduced well rates because higher rates would be possible using this perforation strategy if they were not connected to the manifold. The end result is that the difference in rates between perforating only the laminated layer and perforating both layers in the Popeye simulations in not as high as the difference in rates due to production strategies of the optimization protocol simulations. Therefore, the discounting of reserves in the economics calculations is not going to have as large of an effect on the Popeye simulation results as it does on the optimization protocol simulation results.

Performing the economics calculations on the Popeye simulation results show that it is economic to produce from only the laminated layer of the RN and RM reservoirs (Table 4.8). Even if the discount rate for the economics calculations is increased, it is still economic to produce from only the laminated layer in the RN and RM compartments (Table 3.9). Unfortunately, the optimization protocol does not do a good job of predicting the increases in discounted recovery (*DRPV*) due to only perforating the

laminated layer. Modifications to the simple system used to create the optimization protocol results would need to be made in order to improve its predictive capabilities for the Popeye reservoir.

Reservoir Compartment / Producing Well	*DRPV* (*r* = 7%) For Popeye Results	*DRPV* (*r* = 7%) From Optimization Protocol Results
RN / A3	-5.19	-0.2
RM / A2BP	-9.25	-2.8

Table 3.8: Comparison of economic calculation results for performing economics calculations (*DRPV* and *RPV*, Eq. 2.2 and 2.3, respectively) on results from RN and RM reservoirs at Popeye and on optimization protocol results for the k_{vL}/k_{vM}, k_{hL}/k_{hM} and h_L/h_M conditions that are the same as the RN and RM reservoirs at Popeye (Fig. 3.14B). A 7% discount rate was used for economic calculations (Chapter 3).

Discount Rate	*DRPV* (Recovery Present Value Difference) By Reservoir	
	RM	RN
7%	-9.25	-5.19
10%	-8.16	-4.12
15%	-6.72	-2.85

Table 3.9: Recovery present value difference (*DRPV*) for various discount rates in the *RPV* calculation (Eq. 2.1) for both the RN and RM reservoirs.

Recompleting the A2BP Well (RM Reservoir)

The optimization protocol only considers changing perforation strategies at the onset of production for the field; it does not consider changing perforation strategies at any other time during the life of the field. The Popeye field has been used as an example of how this optimization protocol may have changed initial perforation strategies in a couple reservoir compartments of the Popeye field. Unfortunately, this study has been performed halfway through the predicted production life of the Popeye field and the A2BP well (RM compartment) has already watered out (Fig. 3.11B). Therefore it is

worth looking into the bypassed reserves in the RM as a possible future target for production.

Simulations were performed that changes the perforations in the A2BP well (Fig. 3.1) from both the G_M and G_L being perforated to only the G_L being perforated as soon as water reaches the wellbore in the G_M (water production = 1 STB/D). These simulations show that this strategy effectively produces the bypassed reserves in the laminated layer of the RM reservoir (Fig. 3.15). By recompleting the RM reservoir in only the laminated layer, recovery from the RM reservoir is increased by 19 % (46 BCF).

The results of the recompletion simulations suggest that the optimization protocol would be more robust if the timing of well recompletions could be worked into the protocol. There may be situations that have an increase in recovery due to recompletion but do not show an increase in recovery when only the laminated layer is perforated; there also may be situations where recompleting in the laminated layer at a later time produces more hydrocarbons than if the laminated layer is perforated from the onset of production.

Recompletion could also have a large effect on the economic viability of the different perforation strategies. Recompletion would allow the wells to be produced at the high rates that are possible with both layer of the reservoir perforated and also recover any bypassed reserves by switching to only the laminated layer being perforated. In order to consider recompletion in the economic calculations a whole new economic model would have to be created.

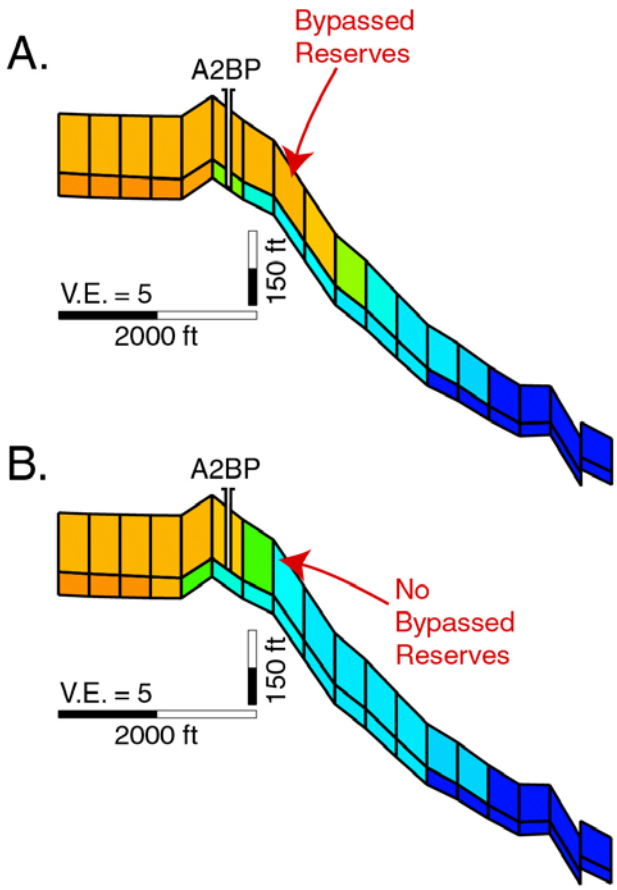

Figure 3.15: Cross-sections through the RM reservoir (A) just before the well is completed in only the laminated layer (April 2001) and (B) after the well is completely shut-in (February 2004). Reserves would be bypassed in the laminated layer if the well was not recompleted but the recompletion allows these reserves to be produced.

Conclusions

Reservoir simulations of the Popeye field predict that perforating both the G_L and G_M of the RA, RN and RM reservoirs will leave bypassed reserves in the laminated layer of the RN and RM compartments. Performing simulations on the Popeye reservoir model with varying perforation strategies show that perforating only the G_L of the A3 (RM) and A2BP (RN) wells and both the G_L and G_M of the A1ST (RA) well would increase the

recovery form the Popeye field by 6% (32 BCF). These changes in recovery compare well with the changes predicted by the optimization protocol for two-layer reservoirs with crossflow.

Despite the reduced well capacity when only the G_L is perforated, producing from only the G_L of the RN and RM compartments is shown to be economically viable using the *DRPV* calculation (Eq. 2.2). Unfortunately, these results do not compare well with economic calculation results from the optimization protocol. The well constraints for the simulations used to create the optimization protocol would have to be modified to include the influence of multiple wells connected to a subsea manifold.

Finally, the optimization protocol could be improved by incorporating well recompletion when water reaches the wellbore in the massive layer as a possible perforation strategy for two-layer reservoirs with crossflow. This has the potential to produce more reserves than perforating the laminated layer from the onset of production. In addition, the economic viability of this strategy may be higher than the other perforation strategies because it is possible to produce at high well rates when both layers are perforated and to produce the additional reserves that would have been bypassed by recompleting in only the laminated layer.

References

Clemenceau, G. R., J. Colbert, and D. Edens, 2000, Production Results from Levee-Overbank Turbidite Sands at Ram/Powell Field, Deep Water Gulf of Mexico: GCSSEPM Foundation 20th Annual Research Conference Deep-Water Reservoirs of the World.

Ehlig-Economides, C. A., and J. Joseph, 1987, A New Test for Determination of Individual Layer Properties in a Multilayered Reservoir: SPE Formation Evaluation, v. SPE 14167, p. 261-283.

Ertekin, T., J. H. Abou-Kassem, and G. R. King, 2001, Basic Applied Reservoir Simulation: SPE Textbook Series, v. 7: Richardson, TX, 406 p.

Holman, W. E., and S. S. Robertson, 1994, Field Development, Depositional Model, and Production Performance of the Turbiditic "J" Sands at Prospect Bullwinkle, Green Canyon 65 Field, Outer-Shelf Gulf of Mexico: GCSSEPM Foundation 15th Annual Research Conference, Submarine Fans and Turbidite Systems, p. 139-150.

Horne, R. N., 1995, Modern Well Test Analysis: A Computer-Aided Approach: Palo Alto, CA, Petroway Inc.

Kucuk, F., M. Karakas, and L. Ayestaran, 1986, Well Testing and Analysis Techniques for Layered Reservoirs: SPE Formation Evaluation, v. SPE 13081, p. 335-41.

Lerch, C. S., K. W. Bramlett, W. H. Butler, J. N. Scales, T. B. Stroud, and C. A. Glandt, 1996, Integrated 3D reservoir modeling at Ram/Powell Field: A turbidite deposit in the eastern Gulf of Mexico: Society of Petroleum Engineers, v. SPE 36729.

Mattax, C. C., and R. L. Dalton, 1990, Reservoir Simulation: Journal of Petroleum Technology, v. SPE 20399, p. 692 - 695.

Pfeiffer, D. S., B. T. Mitchell, and Y. Y. Gilbert, 2000, Mensa, Mississippi Canyon Block 731 Field, Gulf of Mexico - An integrated field study: GCSSEPM Foundation 20th Annual Research Conference: Deep Water Reservoirs of the World.

Rafalowski, J. W., B. W. Regel, D. L. Jordan, and D. O. Lucidi, 1994, Green Canyon Block 205 lithofacies, seismic facies, and reservoir architecture, *in* P. Weimer, and T. L. Davis, eds., AAPG Studies in Geology 42, v. 42: Tulsa, OK, AAPG/SEG, p. 133-142.

Slatt, R. M., G. H. Browne, R. J. Davis, G. R. Clemenceau, J. R. Colbert, R. A. Young, H. Anxionnaz, and R. J. Spang, 1998, Outcrop-Behind Outcrop Characterization of Thin-bedded Turbidites for Improved Understanding of Analog Reservoirs: New Zealand and Gulf of Mexico: Society of Petroleum Engineers, v. SPE 49563.

White, C. D., R. L. Bradburn, R. L. Brown, and M. A. Thieme, 1992, Reservoir potential of thin-bedded turbidites: Prospect Tahoe: 67th Annual Conference and Exhibition of the Society of Petroleum Engineers.

Appendix A

Determination of Rock Properties for the Popeye Reservoir Model

Modeling of Rock Compaction Effects of the G-sand at Popeye

The Popeye compaction model was derived using experiments performed on eight core samples taken from two Popeye exploratory wells in a manner similar to that suggested by Ostermeier (1993). By averaging data for several core samples, a relationship between instantaneous pore compressibility (c_p) and effective stress (σ_v) is developed (Fig. A-1).

The relationship between instantaneous pore compressibility and effective stress can be transformed into a relationship between reservoir pressure and porosity (Φ). The relationship between reservoir pressure and porosity can be used in a simulator to determine how the porosity of the reservoir decreases due to a reduction in fluid pressure.

The pore pressure for a specific effective stress is calculated using

$$\sigma_v = S_v - P_p \ , \qquad \text{A-1}$$

where S_v is the overburden stress and P_p is the pore pressure. Substituting equation A-1 into the equation for a change in porosity due to an incremental change in effective stress

$$\Delta\Phi = -c_p\left(\Phi(1-\Phi)\right)\Delta\sigma_v, \qquad \text{A-2}$$

where Φ is porosity, a change in porosity due to a change in pore pressure can be calculated. The overburden stress of 10,210 psi is taken from Shell Offshore Inc. core reports that contain the compressibility behavior data (Table A-1).

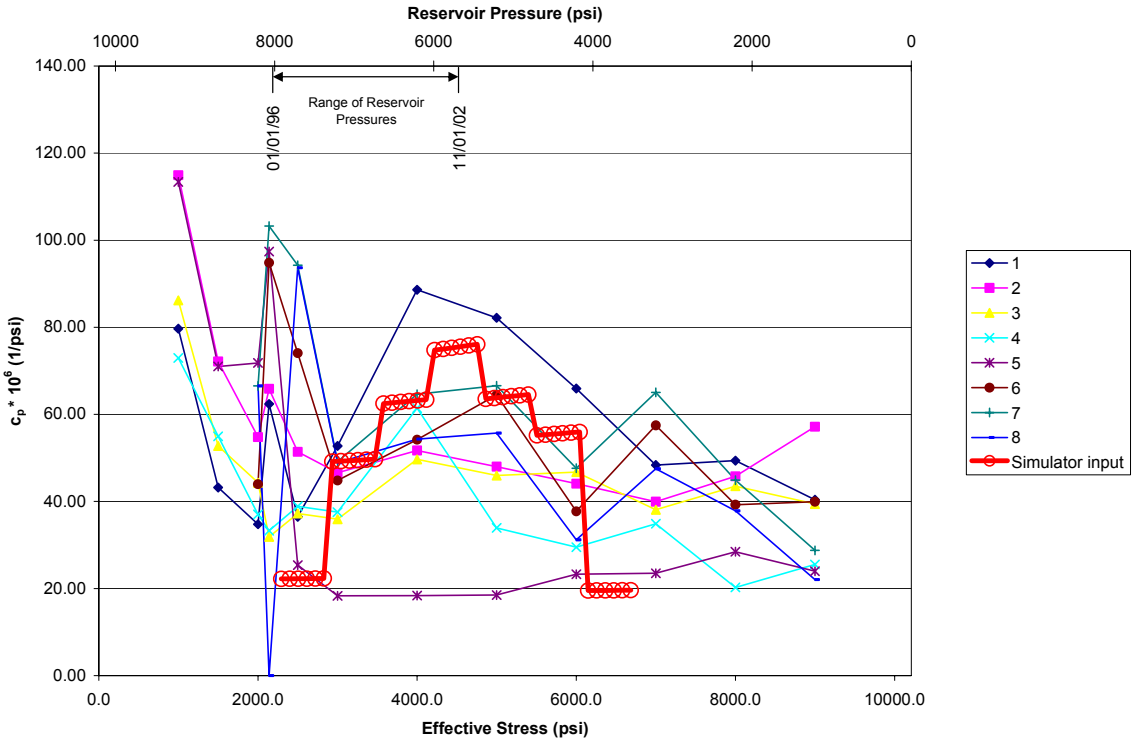

Figure A-1: Effective stress versus instantaneous compressibility for core data taken from Popeye exploratory wells. Samples one through five are from the 116-2 well and six through eight are from the 116-ST3 well. Also includes the table lookup values used in the simulator. Notice that the simulator table lookup follows the behavior of the core samples.

Sv =10210 psi				
P_p (psi)	Φ	ΔΦ	c_p (1/psi)	σ_v (psi)
3525	0.2550	0.0004	1.9628E-05	6685
4168	0.2574	0.0011	5.5974E-05	6042
4811	0.2643	0.0013	6.4575E-05	5399
5454	0.2724	0.0016	7.6107E-05	4756
6096	0.2821	0.0014	6.3394E-05	4114
6739	0.2904	0.0011	4.9700E-05	3471
7382	0.2970	0.0005	2.2324E-05	2828
8025	0.3000	0.0000	0.0000E+00	2185

Table A-1: Table lookup values for pore volume reduction used in simulation. P_p are the values used to interpolate the reduction in pore volume due to a decrease in reservoir pressure. The rest of the table demonstrates the results of calculating the instantaneous pore compressibility. This compaction model is also used any simulations performed using the simple model.

Porosity Assumptions

The reservoir model consists of a laminated sand layer (G_L) overlying a massive sand layer (G_M). The G_L has been assigned an initial porosity of 25% while the G_M has been assigned an initial porosity of 30%. These values are averages taken from core samples of the Popeye exploratory wells (116-2 and 116-2ST3). The porosity is allowed to vary through time based on the compaction model. Assigning the G_L and G_M homogenous properties are considered valid assumptions due to the consistency of the log characteristics throughout the field.

Relative Permeability and Capillary Pressure

Due to the facies difference between the G_M and G_L layers in the reservoir model it is necessary to have a different set of relative permeability curves for each layer. The two-phase relative permeability curves for both oil-water and gas-oil relative permeabilities used in the G_M and G_L were determined by Shell Exploration and Production Company using an internal database of Gulf of Mexico turbidite sands that is based on absolute permeability and fluid content (Figs. A-2 and A-3). In order to determine the three-phase relative permeability, the simulator uses Stone's 2nd model (Stone, 1973).

The capillary pressure relationships were determined by converting mercury-air capillary pressure experiments performed on core samples into oil-water and gas-oil capillary pressure relationships (Fig. A-4). The core samples used in these experiments were from wells 116-2 and 116-2ST3 (Fig. 4.1).

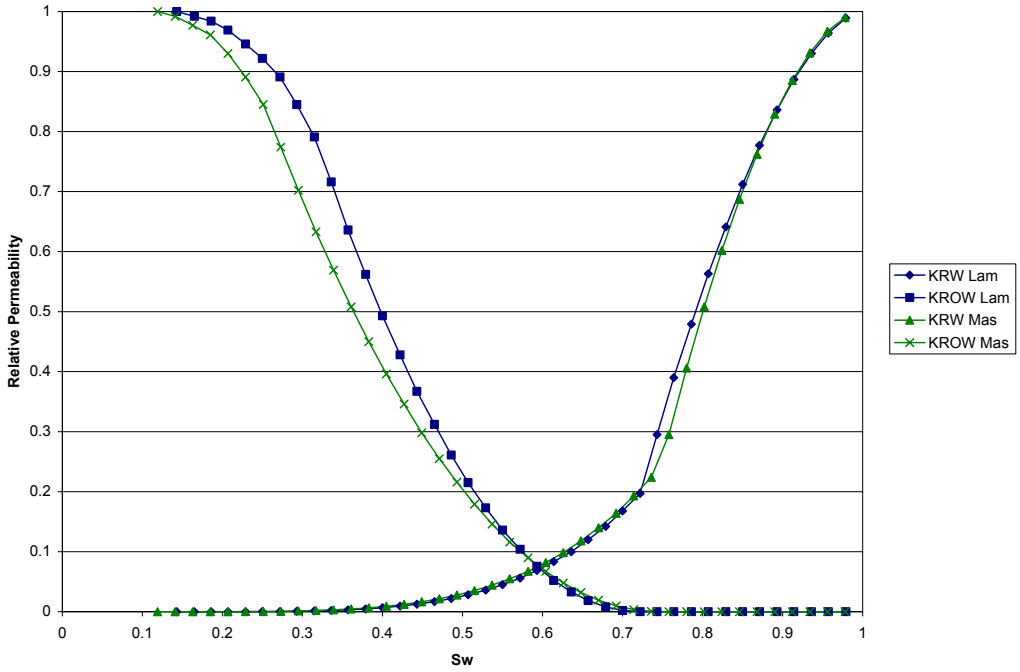

Figure A-2: Water-oil relative permeability curves for both the G_M and G_L layer of the Popeye reservoir model and the laminated and massive layers of the simple model. The same curves are used for both the Popeye simulations and any simulations performed using the simple model.

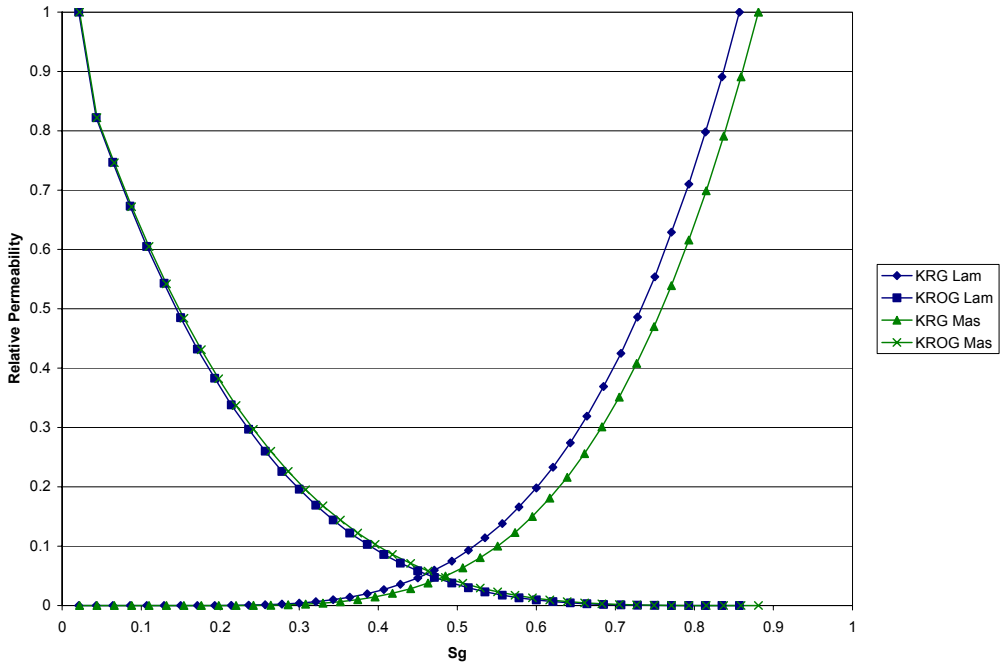

Figure A-3: Oil-gas relative permeability curves for both the G_M and G_L layers of the Popeye reservoir model and the laminated and massive layers of the simple model. The same curves are used for both the Popeye simulations and any simulations performed using the simple model.

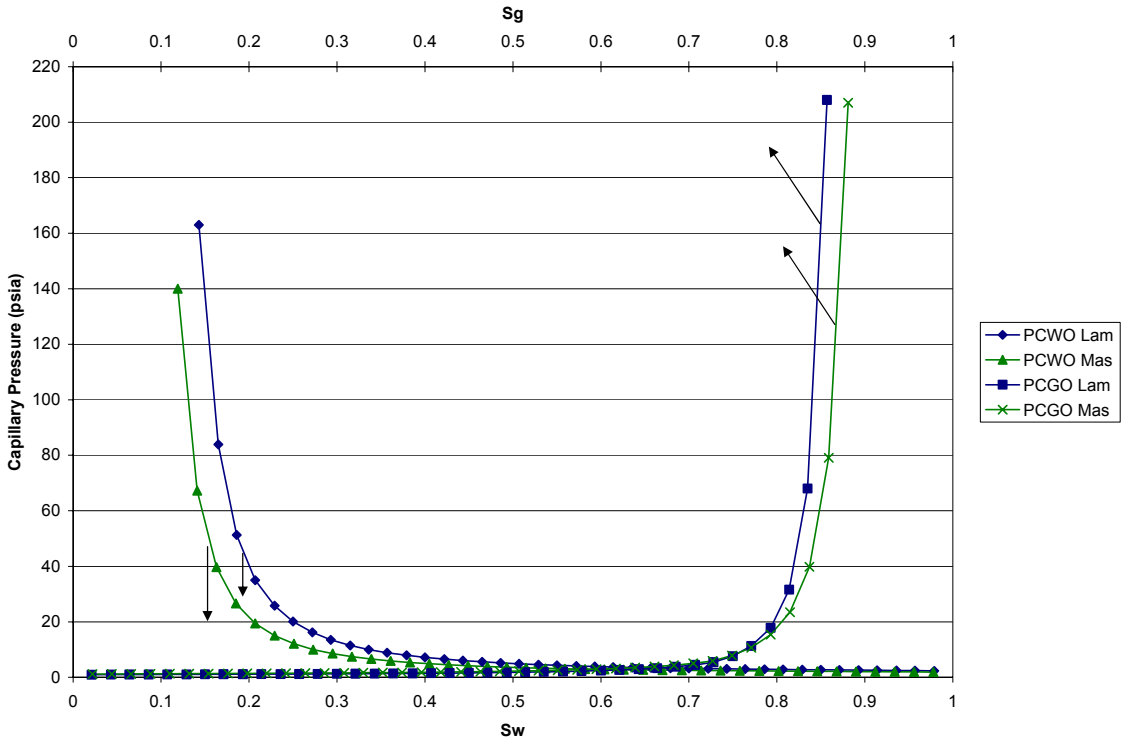

Figure A-4: Water-oil and oil-gas capillary pressure curves for both the G_M (green) and G_L (blue) layers in the Popeye reservoir model and the laminated (green) and massive (blue) layers of the simple model. The same curves are used for both the Popeye simulations and any simulations performed using the simple model.

Gas-Water Contacts (GWC)

There is a separate GWC for each of the four reservoir compartments in the Popeye reservoir simulator (Table A-2). These GWCs are crucial to the history match performed for the Popeye field. A reference pressure of 8398.3 psi and reference depth of 13000 ft. was used to determine the pressure at a reference depth based on the GWC of each reservoir. This ensures that all the reservoir compartments of the Popeye reservoir model are in pressure equilibrium.

Reservoir Compartment	GWC (ft)
RA	11800
RB	11750
RN	12143
RM	11950

Table A-2: Gas-water contacts (GWC) for the reservoirs of the Popeye field.

Modeling of Fluid Properties in the G-sand at Popeye

Three of the four hydrocarbon bearing compartments contain different hydrocarbon compositions and for simulation, the fourth compartment (RB) is assumed to have the same composition as the RA reservoir. In all of the compartments the contents is gas condensate. Several different inputs including molecular weight, critical temperature, critical pressure, critical Z-factor, acentric factor, Peng Robinson Omega A and Omega B factors for each hydrocarbon component and binary interaction coefficients between all the hydrocarbon components are required for each set of PVT data.

Compositional fluid models have been constructed for each reservoir compartment by Shell Exploration and Production Company using the Peng-Robinson (PR) Equation of State (EoS) (Peng and Robinson, 1976). The models are based on PVT samples taken from each of the producing wells in the reservoir compartments. Pseudo-components are created in order to decrease the complexity of the fluid models, which reduces simulation time. Each fluid region has different PVT data (Table A-3 to A-5), however, the same pseudo-components are used for each region. The properties of these components vary slightly in order to better match behavior of the original PVT samples from each compartment.

Fluid properties for GRA/GRB reservoir								
Components	Initial Mole Fractions	MW	T_C (ºF)	P_C (psia)	Z_C	Acentric Factor	Omega A	Omega B
GC1	0.905378	16.062	-116.931	666.067	0.287075	0.011037	0.45724	0.0778
GC2	0.022870	30.906	89.955	729.387	0.286697	0.106561	0.45724	0.0778
GC3	0.036660	58.812	293.285	549.056	0.278173	0.19888	0.45724	0.0778
GC4	0.019690	119.769	565.822	381.749	0.25304	0.402310	0.45724	0.0778
GC5	0.012150	199.526	799.125	285.039	0.252688	0.618184	0.45724	0.0778
GC6	0.003252	305.254	1031.395	219.600	0.251949	0.843152	0.45724	0.0778

Binary interaction coefficients					
	GC1	GC2	GC3	GC4	GC5
GC2	0.04220	-	-	-	-
GC3	0.03758	0.00571	-	-	-
GC4	0.03610	0.00564	0	-	-
GC5	0.03411	0.00554	0	0	-
GC6	0.03151	0.00541	0	0	0

Table A-3: Initial fluid properties used for the RA and RB reservoirs in the Popeye reservoir model. These fluid properties are also used in any simulations performed using the simple model (Chapter 3).

Fluid properties for the GRM reservoir								
Components	Initial Mole Fractions	MW	T_C (ºF)	P_C (psia)	Z_C	Acentric Factor	Omega A	Omega B
GC1	0.953844	16.066	-116.975	666.002	0.2862388	0.011044	0.45724	0.0778
GC2	0.011570	31.2700	89.898	738.857	0.2871132	0.109846	0.45724	0.0778
GC3	0.016400	59.0150	294.077	547.989	0.2777431	0.199342	0.45724	0.0778
GC4	0.009946	120.313	566.921	380.087	0.252873	0.404187	0.45724	0.0778
GC5	0.007143	201.14	799.901	281.737	0.2525793	0.623556	0.45724	0.0778
GC6	0.001097	335.93	1066.022	212.857	0.2659473	0.877766	0.45724	0.0778

Binary interaction coefficients					
	GC1	GC2	GC3	GC4	GC5
GC2	0.03653	-	-	-	-
GC3	0.03083	0.00823	-	-	-
GC4	0.03160	0.00813	0	-	-
GC5	0.03261	0.00799	0	0	-
GC6	0.03464	0.00771	0	0	0

Table A-4: Initial fluid properties used for the RM reservoir in the Popeye reservoir model.

Fluid properties of the GRN reservoir								
Components	Initial Mole Fractions	MW	T_C (ºF)	P_C (psia)	Z_C	Acentric Factor	Omega A	Omega B
GC1	0.958417	16.0621	-116.929	666.070	0.286240	0.011036	0.45724	0.0778
GC2	0.010770	31.7729	89.819	751.958	0.288290	0.114392	0.45724	0.0778
GC3	0.016530	58.9057	293.940	548.525	0.277728	0.199115	0.45724	0.0778
GC4	0.008450	120.968	568.182	378.354	0.253104	0.406292	0.45724	0.0778
GC5	0.004311	194.636	780.964	285.498	0.252489	0.609291	0.45724	0.0778
GC6	0.001522	329.057	1056.543	206.431	0.255913	0.888227	0.45724	0.0778
Binary interaction coefficients								
	GC1	GC2	GC3	GC4	GC5			
GC2	0.03669	-	-	-	-			
GC3	0.02486	0.01178	-	-	-			
GC4	0.01950	0.01163	0	-	-			
GC5	0.01308	0.01146	0	0	-			
GC6	0.00062	0.01111	0	0	0			

Table A-5: Initial fluid properties used for the RN reservoir in the Popeye reservoir model.

Appendix B

Simulations Using Simple Model Performed For Optimization Protocol

Simulation Number	k_{vL}/k_{vM}	k_{hL}/k_{hM}	h_L/h_M
1	0.002	0.02	0.1
2	0.002	0.02	0.5
3	0.002	0.02	1.0
4	0.002	0.02	1.5
5	0.002	0.02	2.0
6	0.002	0.06	0.1
7	0.002	0.06	0.5
8	0.002	0.06	1.0
9	0.002	0.06	1.5
10	0.002	0.06	2.0
11	0.002	0.10	0.1
12	0.002	0.10	0.5
13	0.002	0.10	1.0
14	0.002	0.10	1.5
15	0.002	0.10	2.0
16	0.002	0.21	0.1
17	0.002	0.21	0.5
18	0.002	0.21	1.0
19	0.002	0.21	1.5
20	0.002	0.21	2.0
21	0.002	0.42	0.1
22	0.002	0.42	0.5
23	0.002	0.42	1.0
24	0.002	0.42	1.5
25	0.002	0.42	2.0
26	0.002	0.60	0.1
27	0.002	0.60	0.5
28	0.002	0.60	1.0
29	0.002	0.60	1.5
30	0.002	0.60	2.0
31	0.002	0.83	0.1
32	0.002	0.83	0.5
33	0.002	0.83	1.0
34	0.002	0.83	1.5
35	0.002	0.83	2.0

Simulation Number	k_{vL}/k_{vM}	k_{hL}/k_{hM}	h_L/h_M
36	0.0008	0.02	0.1
37	0.0008	0.02	0.5
38	0.0008	0.02	1.0
39	0.0008	0.02	1.5
40	0.0008	0.02	2.0
41	0.0008	0.06	0.1
42	0.0008	0.06	0.5
43	0.0008	0.06	1.0
44	0.0008	0.06	1.5
45	0.0008	0.06	2.0
46	0.0008	0.10	0.1
47	0.0008	0.10	0.5
48	0.0008	0.10	1.0
49	0.0008	0.10	1.5
50	0.0008	0.10	2.0
51	0.0008	0.21	0.1
52	0.0008	0.21	0.5
53	0.0008	0.21	1.0
54	0.0008	0.21	1.5
55	0.0008	0.21	2.0
56	0.0008	0.42	0.1
57	0.0008	0.42	0.5
58	0.0008	0.42	1.0
59	0.0008	0.42	1.5
60	0.0008	0.42	2.0
61	0.0008	0.60	0.1
62	0.0008	0.60	0.5
63	0.0008	0.60	1.0
64	0.0008	0.60	1.5
65	0.0008	0.60	2.0
66	0.0008	0.83	0.1
67	0.0008	0.83	0.5
68	0.0008	0.83	1.0
69	0.0008	0.83	1.5
70	0.0008	0.83	2.0

Simulation Number	k_{vL}/k_{vM}	k_{hL}/k_{hM}	h_L/h_M
71	0.0004	0.02	0.1
72	0.0004	0.02	0.5
73	0.0004	0.02	1.0
74	0.0004	0.02	1.5
75	0.0004	0.02	2.0
76	0.0004	0.06	0.1
77	0.0004	0.06	0.5
78	0.0004	0.06	1.0
79	0.0004	0.06	1.5
80	0.0004	0.06	2.0
81	0.0004	0.10	0.1
82	0.0004	0.10	0.5
83	0.0004	0.10	1.0
84	0.0004	0.10	1.5
85	0.0004	0.10	2.0
86	0.0004	0.21	0.1
87	0.0004	0.21	0.5
88	0.0004	0.21	1.0
89	0.0004	0.21	1.5
90	0.0004	0.21	2.0
91	0.0004	0.42	0.1
92	0.0004	0.42	0.5
93	0.0004	0.42	1.0
94	0.0004	0.42	1.5
95	0.0004	0.42	2.0
96	0.0004	0.60	0.1
97	0.0004	0.60	0.5
98	0.0004	0.60	1.0
99	0.0004	0.60	1.5
100	0.0004	0.60	2.0
101	0.0004	0.83	0.1
102	0.0004	0.83	0.5
103	0.0004	0.83	1.0
104	0.0004	0.83	1.5
105	0.0004	0.83	2.0

Simulation Number	k_{vL}/k_{vM}	k_{hL}/k_{hM}	h_L/h_M
106	0.0001	0.02	0.1
107	0.0001	0.02	0.5
108	0.0001	0.02	1.0
109	0.0001	0.02	1.5
110	0.0001	0.02	2.0
111	0.0001	0.06	0.1
112	0.0001	0.06	0.5
113	0.0001	0.06	1.0
114	0.0001	0.06	1.5
115	0.0001	0.06	2.0
116	0.0001	0.10	0.1
117	0.0001	0.10	0.5
118	0.0001	0.10	1.0
119	0.0001	0.10	1.5
120	0.0001	0.10	2.0
121	0.0001	0.21	0.1
122	0.0001	0.21	0.5
123	0.0001	0.21	1.0
124	0.0001	0.21	1.5
125	0.0001	0.21	2.0
126	0.0001	0.42	0.1
127	0.0001	0.42	0.5
128	0.0001	0.42	1.0
129	0.0001	0.42	1.5
130	0.0001	0.42	2.0
131	0.0001	0.60	0.1
132	0.0001	0.60	0.5
133	0.0001	0.60	1.0
134	0.0001	0.60	1.5
135	0.0001	0.60	2.0
136	0.0001	0.83	0.1
137	0.0001	0.83	0.5
138	0.0001	0.83	1.0
139	0.0001	0.83	1.5
140	0.0001	0.83	2.0

Simulation Number	k_{vL}/k_{vM}	k_{hL}/k_{hM}	h_L/h_M
141	0.00005	0.02	0.1
142	0.00005	0.02	0.5
143	0.00005	0.02	1.0
144	0.00005	0.02	1.5
145	0.00005	0.02	2.0
146	0.00005	0.06	0.1
147	0.00005	0.06	0.5
148	0.00005	0.06	1.0
149	0.00005	0.06	1.5
150	0.00005	0.06	2.0
151	0.00005	0.10	0.1
152	0.00005	0.10	0.5
153	0.00005	0.10	1.0
154	0.00005	0.10	1.5
155	0.00005	0.10	2.0
156	0.00005	0.21	0.1
157	0.00005	0.21	0.5
158	0.00005	0.21	1.0
159	0.00005	0.21	1.5
160	0.00005	0.21	2.0
161	0.00005	0.42	0.1
162	0.00005	0.42	0.5
163	0.00005	0.42	1.0
164	0.00005	0.42	1.5
165	0.00005	0.42	2.0
166	0.00005	0.60	0.1
167	0.00005	0.60	0.5
168	0.00005	0.60	1.0
169	0.00005	0.60	1.5
170	0.00005	0.60	2.0
171	0.00005	0.83	0.1
172	0.00005	0.83	0.5
173	0.00005	0.83	1.0
174	0.00005	0.83	1.5
175	0.00005	0.83	2.0

Table B-1: Combinations of h_L/h_M, k_{hL}/k_{hM}, and k_{vL}/k_{vM} used for all 175 reservoir models of the optimization protocol. A simulation was run twice with every reservoir model, once with both layers perforated and once with only the laminated layer perforated. All other simulator properties except the ones in this table were held constant for every simple simulation. Table 3.1 specifies the individual property values used to calculate each ratio in this table. Results from simulations performed with the gray reservoir model were used to create Figure 3.9. Figures 3.4, 3.5, 3.8 and 3.9 were created using results from simulations performed with the red reservoir model.

Appendix C

Integration of Geologic Model and Reservoir Simulation, Popeye Field, Green Canyon Block 116

Refer to packet insert.